Wesleyan University The Honors College

Other Worlds: Analyzing the Light Curves of Transiting Extrasolar Planets

by

Emily Leiner
Class of 2010

A thesis submitted to the
faculty of Wesleyan University
in partial fulfillment of the requirements for the
Degree of Bachelor of Arts
with Departmental Honors in Astronomy

Middletown, Connecticut April, 2010

Acknowledgements

Thank you to everyone who has been a part of these last four years, but especially to my parents, who have always believed in me and supported all my endeavors. You made my education possible, and I would not be the person I am today without your love and support. Thank you also to all the friends I've met at Wesleyan. You are like a second family to me, and these past four years could never have been as wonderful without you.

Thank you to all the Wesleyan faculty and staff who have taught me so much, especially everyone in the Astronomy Department without whose expertise and guidance I would have never been able to do this project. An especially big thank you to Seth Redfield, who always went above and beyond the call of duty as a thesis advisor, doing everything from meticulously editing every chapter, to staying late to help with observations, to taking us to Kitt Peak. Looking back on the past two years I cannot believe how much I've learned from you. It has been an invaluable experience I will never forget.

Thank you to everyone in my research group, especially to Erin who was always available to discuss ideas or commiserate after long hours in the office. Thank you also to the rest of the majors and the grads. You are all brilliant people who always made work more fun and often provided me with much needed coffee. I'll miss you all.

This project was made possible by a grant from the Connecticut Space Grant College Consortium, part of the national NASA-funded Space Grant College and Fellowship Program.

Contents

Chapter 1

Introduction

The question of what constitutes a planet is not a simple one. If it is too small its gravity is insufficient to pull it into a spherical shape and it is unable to clear its orbit of planetessimals and is thus classified as an asteroid or dwarf planet. If it is too large it will be able to ignite thermonuclear fusion and is classified as a star. A planet is thus a body orbiting a star that has collapsed to a rounded shape, cleared its orbit of other bodies, is not a satellite, and has not ignited thermonuclear fusion. This mass range includes celestial bodies from a few times smaller than Earth up to around 13 M_J, the mass at which ignition of deuterium burning occurs (Basri & Brown 2006). Extrasolar planets, or exoplanets, are bodies meeting these requirements that orbit stars other than the Sun. The possibility of the existence of planets around other stars has long been suspected, but the existence of such a planet was not confirmed until 1992 when astronomers announced the discovery of planets around a pulsar PSR 1257+12 (Wolszczan 1992). In the 18 intervening years, over 400 exoplanets have been discovered using a variety of techniques.

1.1 Techniques of Detection

1.1.1 Radial Velocity

The majority of known exoplanets (about 80 percent) have been discovered using the radial velocity (RV) method. In a planetary system, both the planet and its host star orbit the system's center of mass, causing the planet to move in a large ($a >> R_*$) orbit and the star to move along a small ($a << R_*$) orbit and thus appear to wobble slightly. This causes a variation in the star's radial velocity, the speed with which it moves towards or away from the observer. This causes a shift in the spectral features of the star due to the Doppler effect (Doyle 2008).

Using spectra to detect slight radial velocity variations has been a highly successful method of planet detection and has been used to discover the vast majority of planets, including the first planet around a solar-type star (Mayor & Queloz 1995). It does have limitations, however. Because the effect of orbiting planets on their host stars is small, it requires a fairly high signal-to-noise spectra and a well characterized instrumental point spread function to detect even the radial velocity variations caused by large (Jupiter mass) planets orbiting close-in to the star (semi-major axes less than 0.1 AU with orbital periods on the order of a few days), and detecting smaller, farther out planets (an Earth-like exoplanet, for example) is much more difficult. Current technologies can give detections down to about 1 m/s. For comparison, a Jupiter-like planet would have a radial velocity amplitude of about 13 m/s, while an Earth-like planet would have an amplitude of about 0.1 m/s (Doyle 2008). As a result, this detection method is biased towards large, close-in exoplanets, with a lower mass detection limit of approximately 0.25

M_J, and is not expected to be able to detect exoplanets similar to Earth any time soon (Bennett et al. 2008).

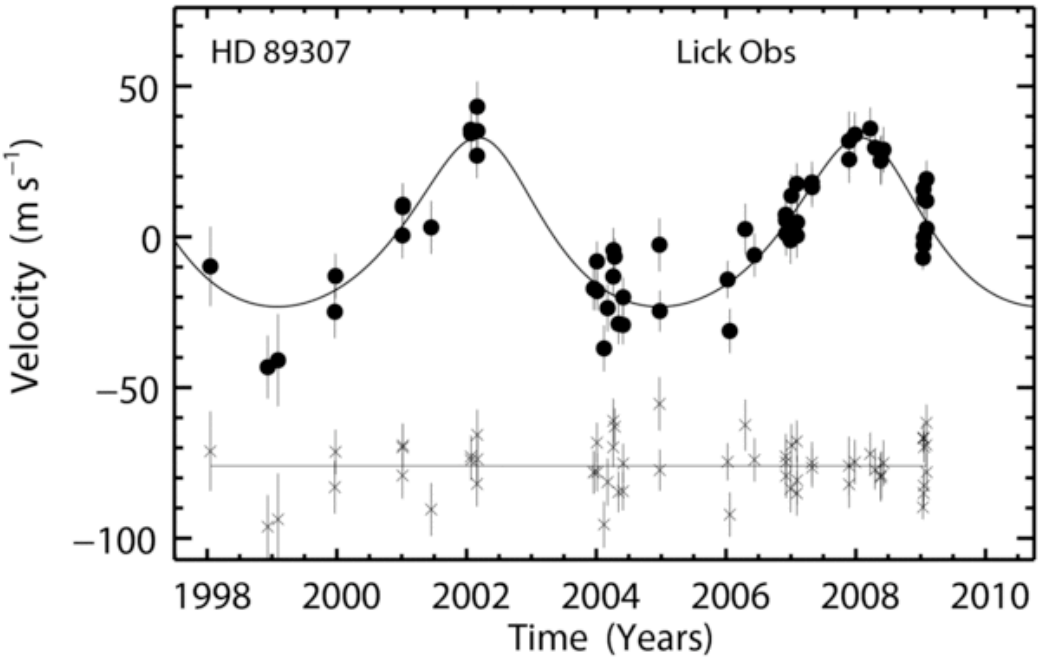

Figure 1.1: A sample radial velocity curve for a HD89207. The radial velocities are from Lick Observatory with a best fit Keplerian model overplotted with a solid line. The radial velocity measurements indicate the presence of a planetary companion with $M \sin i = 1.78 M_J$ (Fischer et al. 2009).

1.1.2 Microlensing

Gravitational microlensing is due to general relativistic effects that cause the gravity of a star to bend the light from a distant background source, magnifying the light like a lens and causing the star to temporarily brighten. If there is a planet orbiting the lensing star, its mass has a measurable impact on the lensing signature. This effect can be quite dramatic. For example, a lensing star at a distance of 5 kpc should have an additional brightening of 4 magnitudes lasting for 5 days if it has a close-in giant planet (3 M_J at a distance of 0.05 AU), or 3

magnitudes lasting for 3 days for a Jupiter-like planet, or 1 magnitude lasting for 4 hours for an Earth-like planet (Doyle 2008).

The chief advantage of this detection method is that it is most sensitive to planets with semi-major axes between 1–5 AU and can detect planets as small as 0.1 Earth masses and no bigger than a few M_J depending on the size of the source star (Beaulieu et al. 2006). This is useful since this is exactly the range within which radial velocity measurements and transit light curves are not very sensitive, and it covers a range of size and orbital distances that could include an Earth-sized planet in the habitable zone (Bennett & Rhie 1996).

The method does have several major drawbacks, however. For one, the lens may be very faint. In addition, gravitational microlensing only occurs when the lensing star and background object are very specifically aligned. This alignment lasts only days or weeks, and after the event ends the lensing observations can never be repeated because the alignment will not occur again. This makes repeating the observation using the microlensing technique impossible, and followups using alternative techniques are also difficult because RV measurements and transits are not sensitive to the range of planetary masses and orbital distances that microlensing can detect. Furthermore, since microlensing events are improbable (the probability of the correct alignment is only about 1 in 10^6 even in the densely packed galactic center), large numbers of stars must be continuously monitored in order to detect such an event (Doyle 2008). Nevertheless, there has been some success using microlensing, and to date 9 planetary systems have been detected using this method (Schneider 2010).

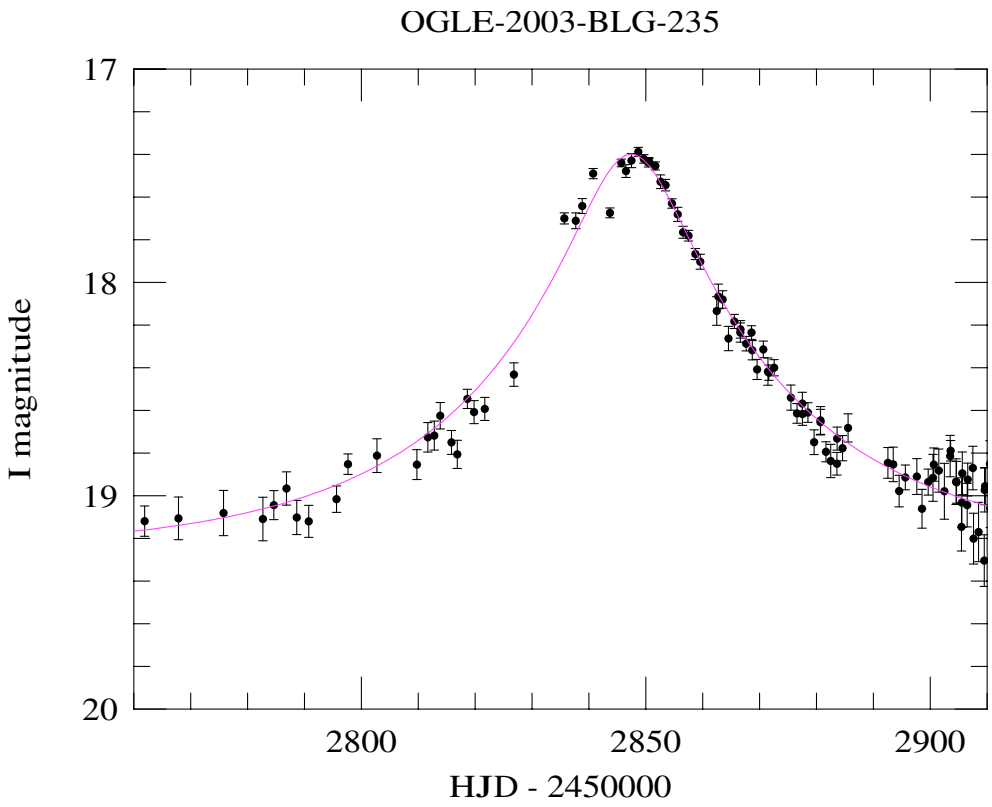

Figure 1.2: A light curve of a microlensing event of the system OGLE-2003-BLG-235. This illustrates a temporary brightening due to the presence of an exoplanet. Data obtained from http://ogle.astrouw.edu.pl/ogle3/ews/2003/blg-235.html

1.1.3 Direct Imaging

In general, it is extremely difficult to detect planets directly, and it is much more common to detect extrasolar planets indirectly using one of the techniques outlined in this section. Planets are very faint compared to their host stars, and the planet's light is generally swamped by the much more luminous star. However, in November 2008, two teams announced independent discoveries of exoplanets via direct imaging. One team discovered 3 planets orbiting the star HR 8799 with masses of 10, 10, and 7 M_J and semi-major axes of 24, 38, and 69 AU (more than twice the separation from the Sun of Saturn, Uranus, and Neptune respectively) using observations from Keck Observatory and Gemini Observatory (Marois et al. 2008). Another team discovered one planet, Fomalhaut b, orbiting at 110 AU with a mass of no more than 3 M_J detected using the *Hubble Space Telescope* (*HST*) (Kalas et al. 2008). This is an amazing triumph of observational astronomy and was only possible with the aid of advanced emerging technologies. The task requires observations from a space-based observatory like *HST*, or large (8–10 m) ground based telescopes equipped with adaptive optics such as Keck or Gemini, as well as specialized equipment such as a coronagraph designed to block out the light from the host star that otherwise drowns out the signal from the planet, artificially suppressing scattered and diffracted light (Kalas et al. 2008). Even using this cutting-edge technology, direct imaging has so far only resolved enormous gas giants with huge orbital separations from their host stars. Additionally, direct imaging is best used around relatively young systems whose potential planets are still radiating formation heat. Fomalhaut, for example, is only an estimated 100-300 million years old (Kalas et al. 2008). A direct image of Fomalhaut b is given in Figure 1.3.

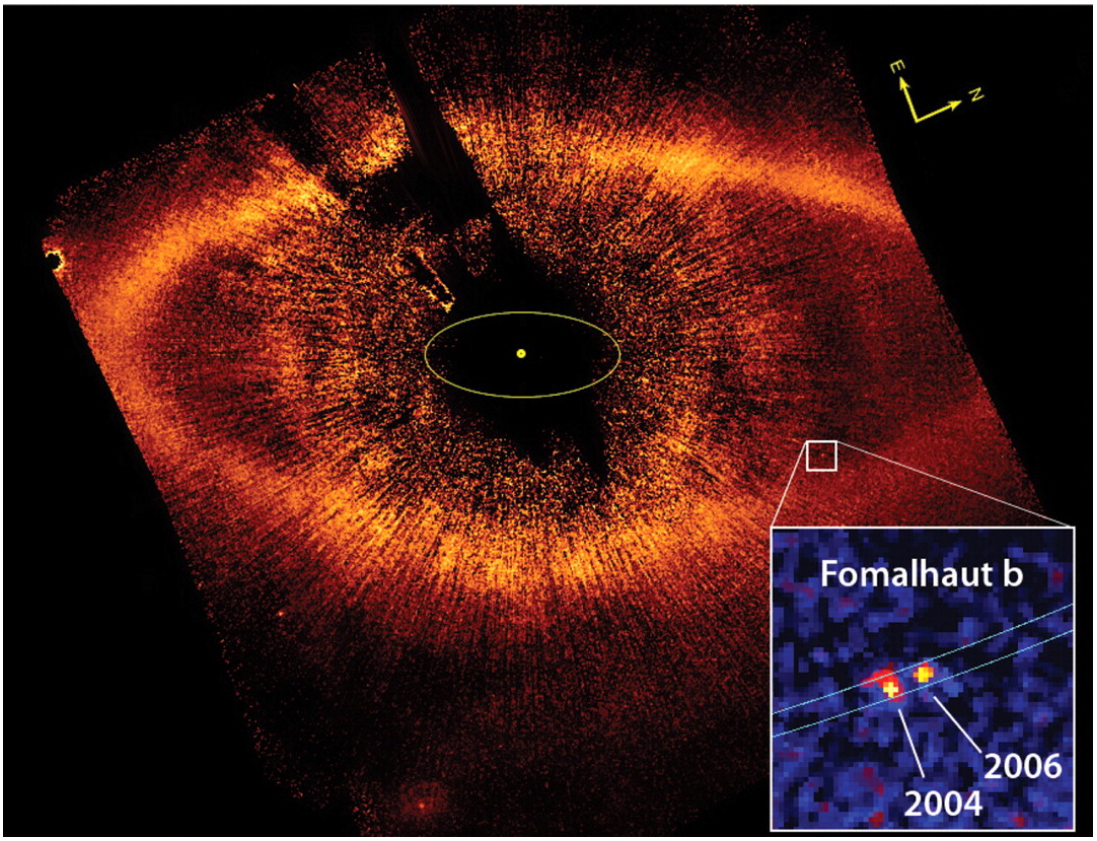

Figure 1.3: A coronagraphic image of Fomalhaut b taken with HST from Kalas et al. (2008). The white square indicates the location of Fomalhaut b, the exoplanet. The other apparent objects are actually galaxies or false positives and the yellow circle is the location of the star, though the star itself is not visible because it is occulted by the coronograph. The yellow ellipse corresponds to the orbit of Neptune in our solar system. The inset is a composite image showing the location of the planet in 2004 and 2006 relative to the host star.

1.1.4 Pulsar Timing Variations

The first confirmed extrasolar planets were detected using the pulsar timing method (Wolszczan 1992). Pulsars emit radio jets, so as the star rotates the radio signal appears to pulse. Any timing anomaly in its radio pulse, then, indicates a slight change in its rotation, and this in turn can indicate the presence of a planet. Pulsar timing is extremely precise, so this method is sensitive to planets far smaller than any other detection method, capable of detecting objects even less massive than Earth (Doyle 2008). However, pulsars are rare objects, and a pulsar with a planet is even rarer. Even if a planet does survive the final stages of stellar evolution that precede the creation of the pulsar, the environment is plagued by intense radiation that would make the prospect of life on such a planet, at least life as we understand it, impossible. This detection method is therefore not the most promising means of discovering a potentially habitable planet, a goal that is one important long-term aim of exoplanet research.

1.1.5 Transit

A transiting exoplanet is a planet around another star that periodically passes in front of its parent star, temporarily dimming the parent star's magnitude. The photometric detection of such a dip in a star's observed brightness is one commonly used method to search for exoplanets. The first detected transiting exoplanet was HD209458 reported by Charbonneau et al. (2000). At that time, 24 exoplanets had already been detected using other methods. Since then, the total number has grown to well over 400, and more than 60 of these planets have been detected using the transit method (Schneider 2010).

The amount of light blocked by a transiting planet can be measured as a

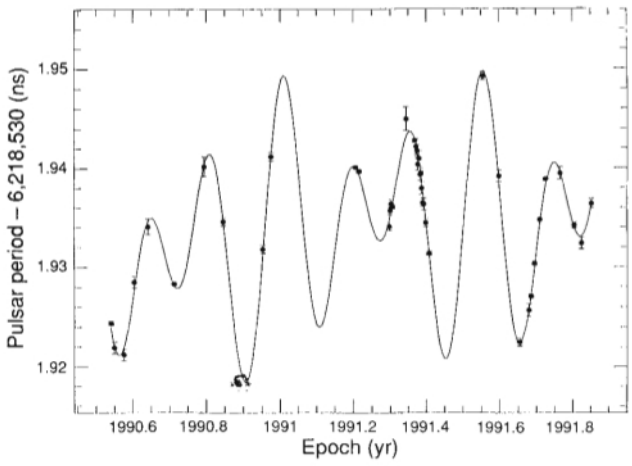

Figure 1.4: Pulsar period variations of the system PSR 1257+12 from Wolszczan (1992). The points are measurements of the pulsar's period; the overlaid solid line is the predicted changes in period if the pulsar is being orbited by two planets with masses $2.8M_{\oplus}$ and $3.4M_{\oplus}$ at distances from the pulsar of 0.47 AU and 0.36 AU respectively. It has been suggested there may also be another, smaller, moon-sized planet at an even smaller distance (Wolszczan 1992).

function of time. From the depth and shape of this light curve it is possible to determine the relative sizes of the star and the planet, the orbital inclination, and the stellar limb-darkening coefficients. When combined with radial velocity measurements, transit data can determine the planetary mass, stellar radius, and thereby also the planetary density. Spectra taken of a transiting planet can also be used to detect the presence of different elements in the planet's atmosphere (Charbonneau et al. 2002). A high-precision light curve can be obtained with even a small ground-based telescope, and thus much information about the system can be gleaned from relatively easy and inexpensive observations.

The transit method of detecting exoplanets has the drawback that it can only detect systems with orbital planes oriented close to edge on, an inclination of at least 80°. Additionally, the method is biased towards detecting giant close-in planets with orbital periods of just a few days. This is because it is easiest to

detect the planets that block the largest portion of light during transit–either planets that are large, or close to their host stars, or both. Additionally, a planet with a close-in orbit has a smaller orbital frequency, a periods of just a few days, allowing a transit to be observed without monitoring the star for a long period of time. For this reason, transiting exoplanets tend to have semi-major axes of approximately 0.01– 0.06 AU with masses between about 0.5 M_J and 10 M_J (Schneider 2010).

Nevertheless, the transit method has the advantage of being one of the most sensitive methods of detecting exoplanets and can provide astronomers with a great deal of information from relatively simple measurements. For this reason, many groups such as TrES, OGLE, HAT, and WASP have used simple ground based telescopes to conduct searches for exoplanets with great success (see O'Donovan et al. 2006; Snellen et al. 2009; Bakos et al. 2009; West et al. 2009 for example), and groups like CoRoT have used space based instruments to search for transiting planets (Léger et al. 2009). An important development in transiting exoplanet research was the launch of *Kepler* in 2009, a space based observatory dedicated specifically to looking for transits. *Kepler* is capable of monitoring thousands of stars at a time. It has the sensitivity to detect Earth-sized planets occupying the habitable zone of sun-like stars, and over the course of its three-and-a-half year mission should return many high-precision light curves that will tell us much about the types of exoplanets out there (Borucki et al. 2010). *Kepler* is just beginning to return data, and the years ahead promise to be an exciting time for exoplanet research, particularly the field of transiting exoplanets.

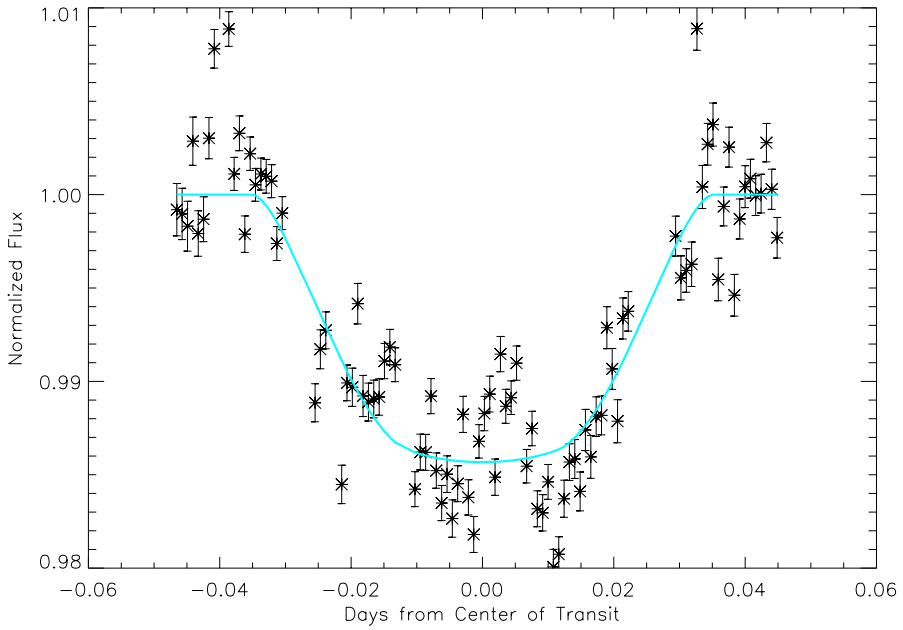

Figure 1.5: Transit light curve for TrES-2 with a fit line overlaid in blue. Data obtained from Wesleyan University's Van Vleck Observatory.

1.2 Transits

1.2.1 The Transit Light Curve

The transit method of detecting exoplanets is remarkable in that much can be learned about an exoplanetary system using remarkably simple observations, just a time series of exposures from which the relative flux of a star can be calculated and a dip in the total flux detected at the time of transit. An example of a transit light curve can be seen in Figure 1.5.

There are four key points in a transit referred to as 1st–4th contact. A diagram of these points is shown in Figure 1.6. First contact begins when the leading edge

of the planet just touches the edge of the star (labeled "1st" in Figure 1.6). This is the point at which the transit begins. Second contact occurs as the planet passes fully in front of the star and the trailing edge of the planet just touches the edge of the star (marked "2nd" in Figure 1.6). After 2nd contact, the planet is fully in front of the star. Third contact is the point at which the leading edge of the planet just touches the far edge of the star (marked "3rd" in Figure 1.6). After this point, the planet is no longer fully in front of the star. Fourth contact occurs as the trailing edge of the planet touches the far edge of the star, the last moment that the planet is occulting the star at all (marked "4th" in Figure 1.6). The transit ends after fourth contact. These important points naturally divide a transit into 4 distinct stages.

1) Ingress, the time between first and second contact when the planet is only partially in front of the star. This is the phase at which the planet is moving in front of the star, blocking more and more light as it travels. A planet in ingress corresponds to point B in Figure 1.8. The corresponding section of the light curve is the portion in which the flux is quickly decreasing marked in Figure 1.7.

2) Egress, the time between third and fourth contact when the planet is only partially in front of the star. Here the planet is moving out from in front of the star, blocking less and less light as it moves. Egress corresponds to that point marked D in Figure 1.8. This corresponding portion of the light curve is the section during which flux is quickly increasing marked in Figure 1.7.

3) Full eclipse, where all of the planet is in front of the star. This occurs between second and third contact, the point marked C in Figure 1.8. This phase corresponds to the bottom of the dip of the light curve labeled "full eclipse" in Figure 1.7 where the flux is not increasing or decreasing as dramatically as during ingress and egress.

4) No eclipse, where the planet does not block any light from the star. This happens before first contact, when the transit has not yet begun, or after 4th contact, when the transit has ended. These points are marked on Figure 1.8 as points A and E. The corresponding portion of the transit light curve is marked in Figure 1.7.

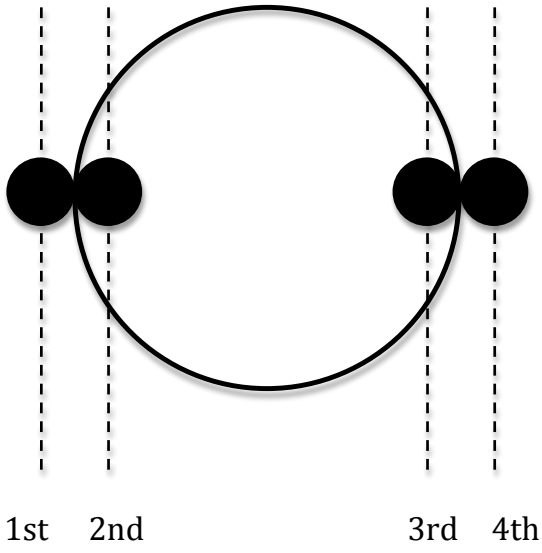

Figure 1.6: A diagram of a transit with 1st through 4th contact labeled.

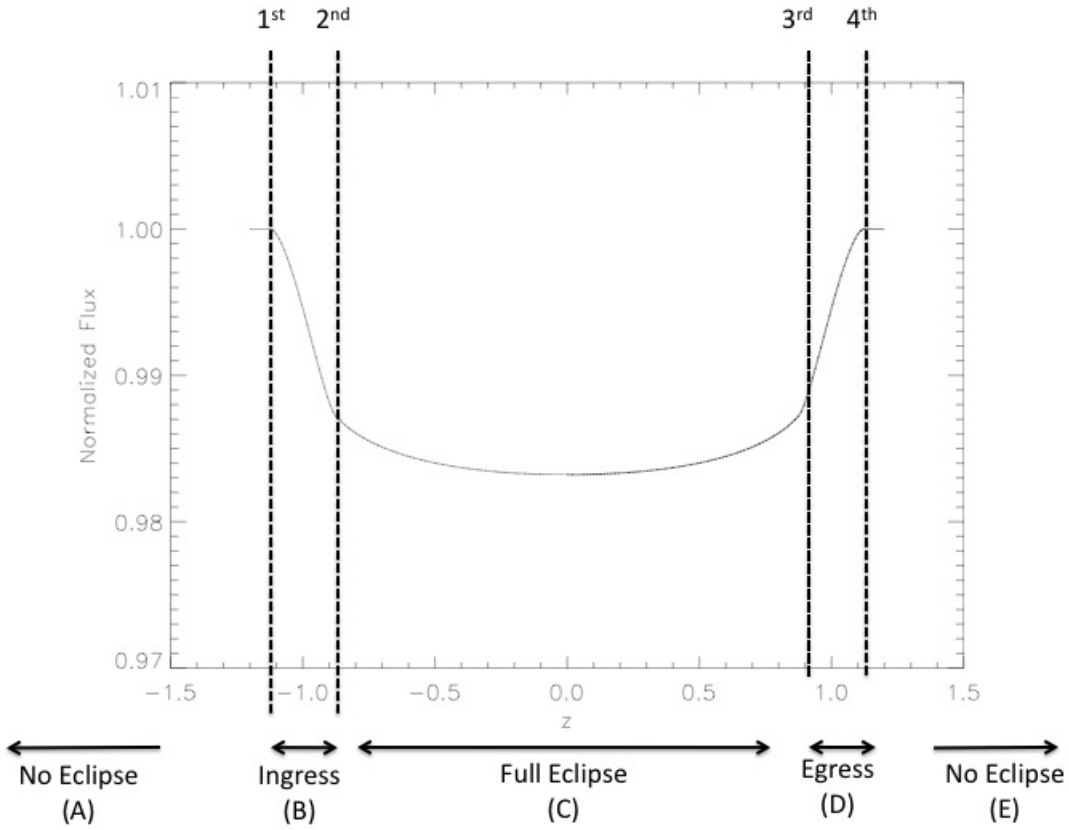

Figure 1.7: A diagram of a transit light curve with each section (no eclipse, full eclipse, ingress and egress) labeled. 1st, 2nd, 3rd, and 4th refer to 1st–4th contact. See Section 1.2.1 for a full discussion of these terms, as well as Figure 1.8 and Figure 1.6.

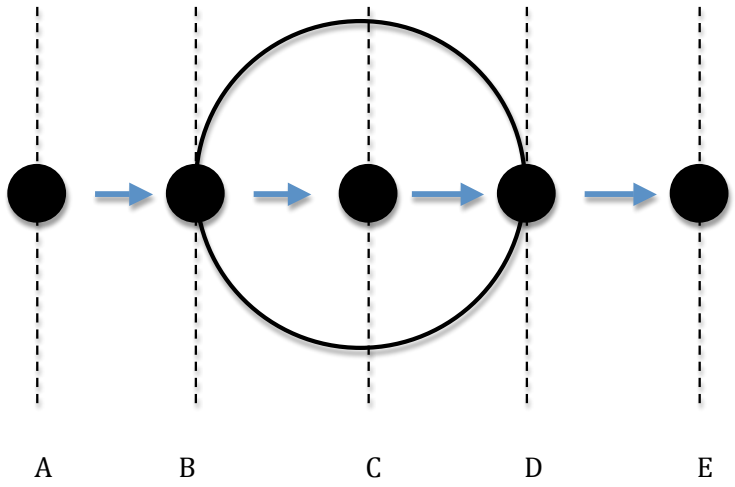

Figure 1.8: A is the time before first contact when the planet is out of transit. B is the time between first and second contact where the planet is partially in front of the star, but not yet blocking the maximum amount of light. C is the time between 2nd and 3rd contact when the planet is fully in front of the star. D is the time between 3rd and 4th contact during which the planet is moving out from in front of the star and is again only partially in front of the star. E is the time after 4th contact when the planet is again out of transit.

1.3 Transiting Exoplanets at Wesleyan

Of all these possible methods of exoplanet detection, the transit method lends itself most easily for use at Van Vleck Observatory at Wesleyan University. Wesleyan has a 24", ground based Perkins telescope with a thermal-electrically cooled 2048×2048 charge coupled device (CCD). This set-up is well suited to doing photometry of stars, the only measurement necessary to construct a transit light curve, but it does not have a spectrograph to obtain radial velocity data, the high-resolution imaging and coronagraph used for direct imaging, nor the ability to monitor the millions of stars simultaneously that microlensing requires. Van Vleck, then, is best suited to detecting planets using the transit method, a highly successful method of detection even with a limited amount of equipment.

The aim of this project was to put in place the measures required to successfully obtain and analyze a transit light curve using Wesleyan's facilities. This included testing the limitations of the 24" telescope and experimenting with various observational procedures, as well as designing and implementing a data reduction procedure that would produce a viable transit light curve, and writing a fitting program that could successfully determine the relative size of the star and planet, the orbital inclination, and the stellar limb-darkening coefficients in addition to identifying transit timing anomalies that might indicate the presence of another planet in the system. I started by designing a transit fitting program (see Chapter 2) that fits a transit light curve to a set of best-fit planetary system parameters. I tested this program for accuracy by comparing fits produced by this program to fits produced in the literature (see Chapter 3). I then selected exoplanet targets to view with the Perkins Telescope. I was able to obtain one useable transit light curve of the exoplanet TrES-2 (See Chapter 4), demonstrating that it is possible

to obtain quality data at Van Vleck Observatory and analyze this data using the reduction programs and the fitting program we designed.

Chapter 2

Light Curve Modeling

In order to gain information on the transiting exoplanet being observed and its host star, it is necessary to fit an observed transit light curve to a theoretical model light curve in order to determine the planetary radius, stellar radius, inclination of the system, ephemeris of the transit, and limb darkening coefficients. The greatest challenge in doing this is choosing a mathematical description of the limb darkening. A full treatment of four different expressions for limb darkening is given in Mandel & Agol (2002), including a uniform source (no limb darkening), a quadratic limb darkening law, a limb darkening approximation for small planets, and a nonlinear limb darkening law. For this project, all but the nonlinear law come into play. Additional information on the limb darkening models of Mandel & Agol (2002), including their computer code, can be found on their website[1].

2.1 Limb Darkening

When modeling an exoplanet transit, it is important to take into account the fact that a star is not uniformly bright across its entire surface. An effect called limb darkening causes the edges of a star to appear darker than the center. Limb darkening results from the fact that the optical depth is different at the edges of the star than at the center. A star becomes opaque at a specific optical depth

[1] http://www.astro.washington.edu/agol

which is uniform across the star, but the radius at which this optical depth is reached increases towards the edge of the star, and thus one cannot see as deep into the solar atmosphere near the edge (for a diagram of this geometry see Figure 2.1). This means that the density and effective temperature of the star appears to diminish towards the edge causing the edge to appear dimmer. Due to limb darkening, a transiting planet will block more light as it transits the center of the star than when it passes in front of the edges. Thus, the limb darkening must be taken in to account when attempting to fit a model light curve to transit data. The limb darkening can be mathematically modeled in several ways. In this section I describe the treatments of limb darkening we used for this project, three of the laws given in Mandel & Agol (2002).

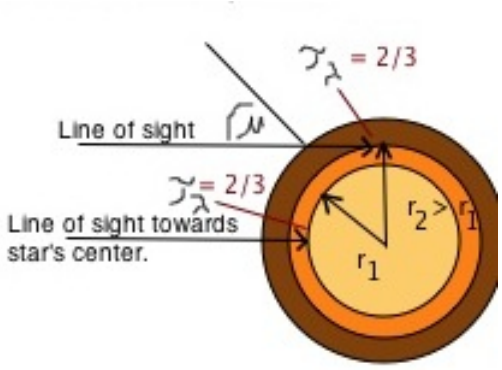

Figure 2.1: A figure describing limb darkening taken from Carroll & Ostlie (2007). The figure illustrates that, when looking towards the edge of the limb, the same optical depth (indicated on the diagram as τ_λ) corresponds to a different point in the stellar atmosphere than when looking straight on. This means that if you look at the center of the star, you see to a deeper, and thus hotter and brighter, layer than if you look towards the edge. This is the effect of limb darkening.

2.1.1 Linear, Non-Limb-Darkened Law

The linear, non-limb darkened law is the most basic. It assumes uniform flux across the entire star and splits the transit into four parts: full eclipse, no eclipse, ingress, and egress. These transit sections are discussed fully in Section 1.2.1. See Figures 1.6–1.8 for illustrations.

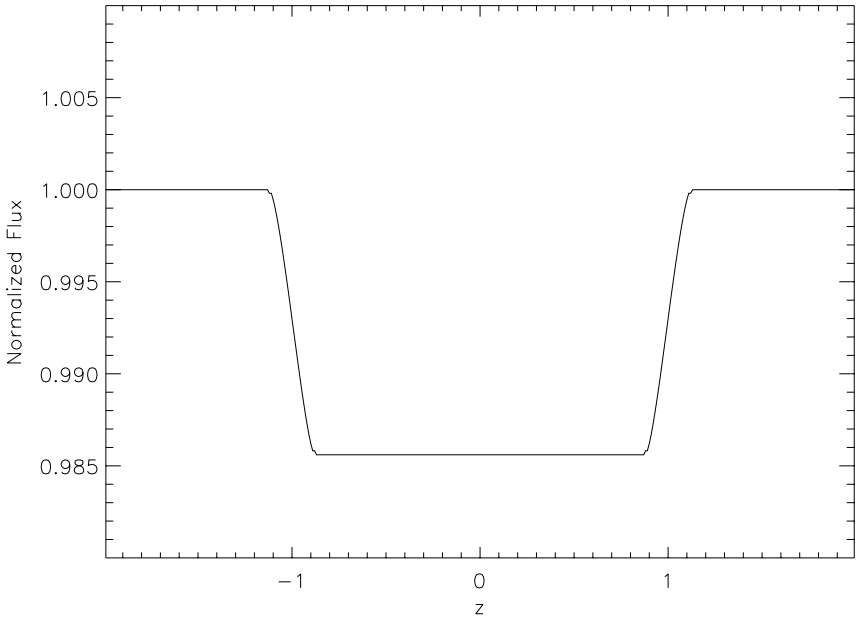

Figure 2.2: A non-limb-darkened light curve generated using the uniform source expressions as given in Mandel & Agol (2002). This assumes $p = R_p/R_* = 0.12$. The x-axis is the impact parameter (z). The y-axis is normalized flux. For the uniform source law, $Flux = 1 - \lambda^e(p, z)$ where λ^e is given in Equation 2.1.

Applying the equation for a uniform source from Mandel & Agol (2002), the only input parameter required is p, the ratio of the radius of the planet (R_p) to the radius of the star (R_*). This law will then generate a light curve with normalized

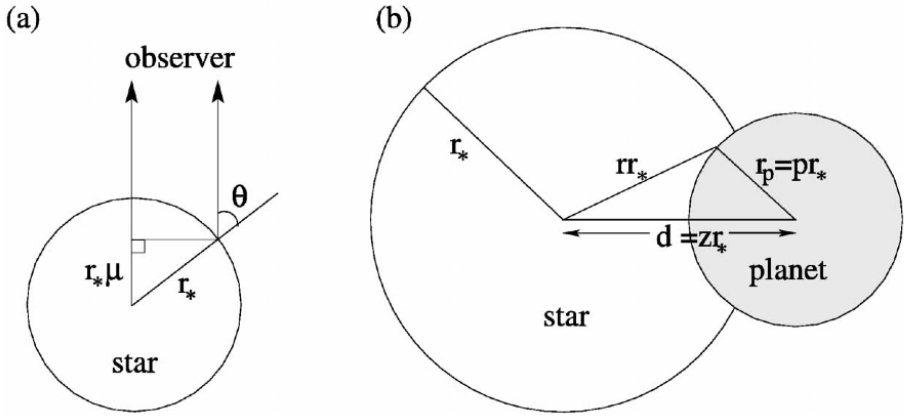

Figure 2.3: The geometry of limb darkening taken from Mandel & Agol (2002). (*a*) This is an edge on view of the star with the observer off the top of the page. The radius of the star is r_*, and θ is the angle between the observer and the normal to the star's surface, and $\mu = \cos\theta$. (*b*) This is the geometry of the transit from the observer's point of view. Note that r_p is the radius of the planet, d is the separation between the center of the star and the center of the planet, and z is known as the impact parameter.

flux $(1 - \lambda^e(p, z))$ as a function of impact parameter (z). The impact parameter is a measure of the separation between the center of the star and the center of the planet. In mathematical terms, $z = R_*/d$ where d is the separation of centers. See Figure 2.3 for an illustration. The equations from Mandel & Agol (2002) that describe this uniform source limb darkening are as follows:

$$\lambda^e(p,z) = \begin{cases} 0, & \text{if } 1+p < z \\ \frac{1}{\pi}[p^2\kappa_0 + \kappa_1 - \sqrt{\frac{4z^2-(1+z^2-p^2)^2}{4}}], & \text{if } |1-p| < z \leq |1+p| \\ p^2, & \text{if } z \leq 1-p \\ 1, & \text{if } z \leq p-1 \end{cases} \tag{2.1}$$

where

$$\kappa_1 = \cos^{-1}\left(\frac{1-p^2+z^2}{2z}\right) \tag{2.2}$$

$$\kappa_0 = \cos^{-1}\left(\frac{p^2+z^2-1}{2pz}\right) \tag{2.3}$$

where z is the impact parameter, $p = \frac{R_p}{R_*}$ and λ^e describes the amount of obscured flux. The λ^e term is related to the normalized flux by $F = 1 - \lambda^e(p, z)$.

The first case in Equation 2.1 (when $1 + p < z$) describes the out of transit flux of the system. The second case describes the flux during ingress and egress (that is, between 1st and 2nd contact, or between 3rd or 4th contact respectively). The third case describes the flux during full eclipse between 2nd and 3rd contact. The fourth case is the situation in which the planet is large enough to occult the entire star at once. This case is not relevant for exoplanets. For a full discussion of this terminology (ingress, 1st–4th contact, etc) see Section 1.2.1 and the figures therein. Note that the 1st, 3rd, and 4th cases are actually special cases of the 2nd case. The 2nd case reduces to the 1st case at $z = 1 + p$, to the 3rd case at $z = 1 - p$, and to the 4th case at $z = 1 - p$.

Figure 2.2 shows a light curve using this uniform source approximation. This light curve gives a general impression of the magnitude of the eclipse, but because it does not take into account the limb darkening it is flatter than an actual transit curve. This is because the limb darkening causes the planet to block more light if it is close to the center of the star than if it is on the edge, so the dip in the curve will not have a flat bottom. Instead it will curve down slightly more until it reaches the center, where it blocks the maximum light, and then begins to curve back upward. This is the shape the curves take in Figures 2.4 and 2.6 when the limb darkening is considered.

2.1.2 Small Planet Approximation

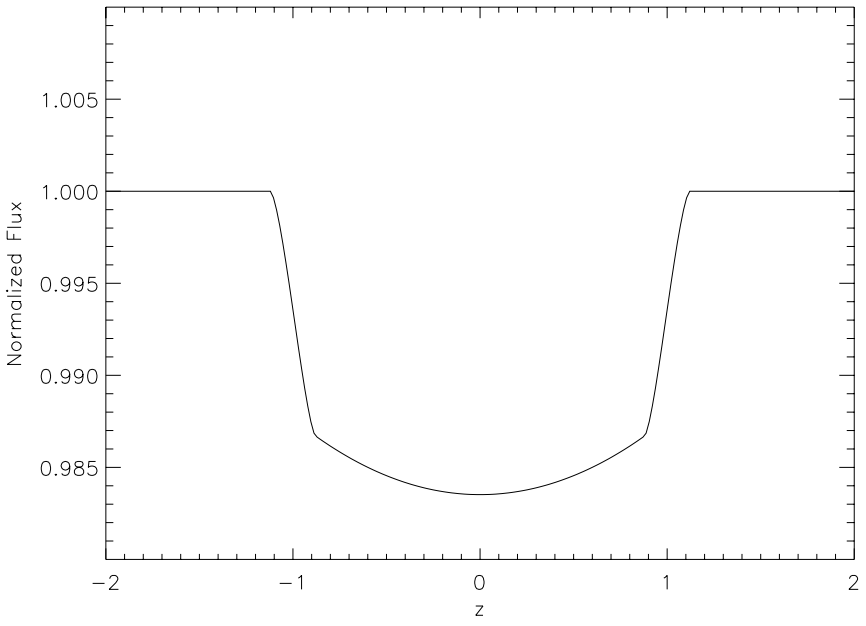

Figure 2.4: Light curve generated using the small planet approximation for limb darkening as given in Mandel & Agol (2002) assuming $p = 0.12$.

If the transiting planet is small relative to its host star the interior of the light curve can be approximated by assuming that the surface brightness of the star is constant across the area eclipsed by the planet. The interior of the transit is defined as $z < 1-p$. This approximation works for $p \leq 0.1$ (Mandel & Agol 2002). There are many systems with small enough p values to use this approximation. Out of the 10 transiting systems with the brightest V-band apparent magnitudes, 8 have p values small enough to use this approximation (see Table 2.1).

I uncovered an error in the expression for $I^*(z)$ given in Mandel & Agol (2002).

Planet Name	p	V-mag
HD 209458	0.12	7.65
HD 189733	0.148	7.67
HD 149026	0.045	8.15
HD 17156	0.073	8.17
HAT-P-2	0.069	8.71
WASP-7	0.076	9.51
HAT-P-11	0.060	9.59
WASP-14	0.100	9.75
XO-3	0.091	9.8
HAT-P-8	0.098	10.17

Table 2.1: The 10 transiting systems with the brightest V-band apparent magnitude. Of these 10 transiting systems, 8 have $p < 0.10$, small enough to use the small planet approximation of Mandel & Agol (2002). These value are taken from the Exoplanet Encyclopedia (Schneider 2010).

Using Mandel and Agol's original expression for $I^*(z)$ produces a light curve with an elongated period of ingress and egress. These sections are stretched by a factor of π (see Figure 2.5). Therefore, I determined that the expression should be:

$$I^*(z) = (\pi - \pi a)^{-1} \int_{z-p}^{1} I(r) 2r dr \tag{2.4}$$

where $a = (z-p)^2$, $I^*(z)$ is the specific intensity as a function of z and $I(r)$ is the specific intensity as a function r, and r is the normalized radial coordinate on the star. This $I^*(z)$ can be related to flux through Equation 8 of Mandel & Agol (2002) (given as Equation 2.5 here) in order to produce a light curve.

$$F = 1 - \frac{I^*(z)}{4\Omega}[p^2 \cos^{-1}(\frac{z-1}{p}) - (z-1)\sqrt{p^2 - (z-1)^2}] \tag{2.5}$$

The small planet approximation produces a curve significantly more curved than the uniform source model (given in Figure 2.2) since it takes the limb darkening into account. A sample light curve generated using the small planet ap-

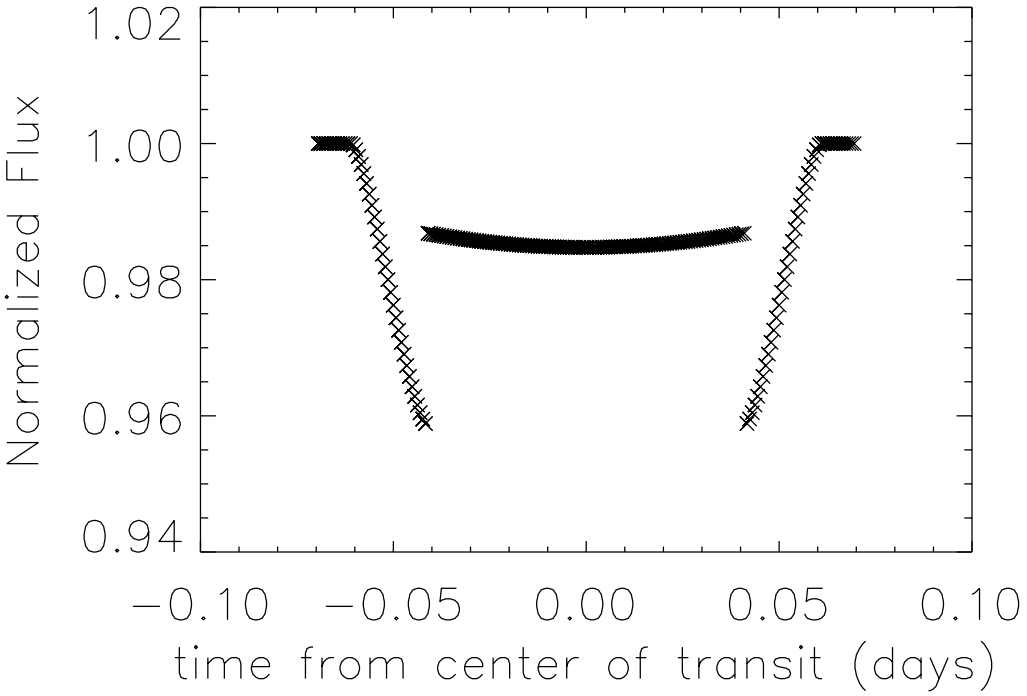

Figure 2.5: Light curve for HD209458 using a small planet approximation without the additional factor of $1/\pi$ given in Equation 2.4. Without this factor, the periods of ingress and egress are clearly stretched out by a factor of about 3.

proximation is given in Figure 2.4.

2.1.3 Quadratic Limb-darkening

For planets with $p > 0.1$, assuming the surface brightness to be uniform under the planet is no longer acceptable, and a more sophisticated treatment of the limb darkening is required. This model utilizes the quadratic limb-darkening functions described by Mandel & Agol (2002). Revised versions of these equations are given

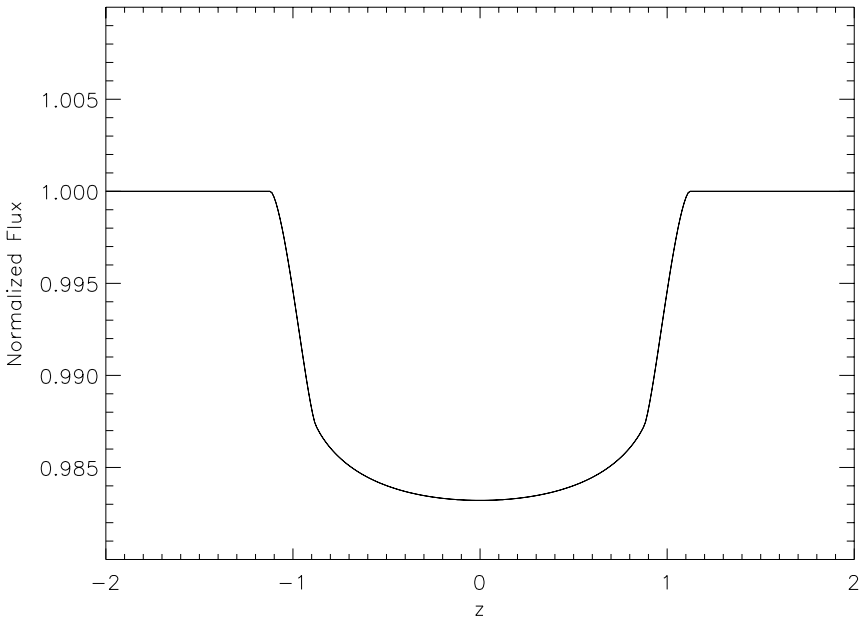

Figure 2.6: Light curve generated using the quadratic limb darkening law as given in Mandel & Agol (2002)

in Table 2.2 and Equations 2.6–2.13. This revised table is necessary because there are a few errors in the expressions as given by Mandel & Agol (2002), and therefore the following corrections and modifications are required. For definitions of z and p see Section 2.1.1. A definition of k is given in Equation 2.14.

1) If $z < p$, $\frac{2}{3}$ must be added to λ_d. Without this additional term, the center of the light curve will be off, underestimating the flux at the center of transit by exactly $\frac{2}{3}$. This change is reflected in case 14 in Table 2.2.

2) In the equation for λ_3, it is useful to substitute $\frac{1}{2p}$ into the complete elliptic integrals instead of $\frac{1}{2k}$. This avoid errors when computing limb darkening at $p = z$ and still yields the correct values. The correct expression for λ_3 is listed in

Equation 2.8.

3) In the equation λ_4, it is useful to substitute $2p$ in for $2k$ in the expressions for the elliptic integrals. Again, this avoids errors when computing limb darkening at $p = z$. The correct expression is listed in Equation 2.9.

4) In the equation for λ_5, it is necessary to multiply by an additional factor of $\sqrt{p - p^2}$. The correct expression is given in Equation 2.10

5) An additional case must be considered for $|p + z - 1|$ close to zero. For more discussion, see Section 2.1.4. This additional case is reflected in cases 12 and 13 in Table 2.2.

The quadratic law gives a light curve that is smoother and more rounded than either the uniform source law or the small planet approximation (given in Figure 2.2 and Figure 2.4 respectively) since it takes into account an even more detailed treatment of the limb darkening. Essentially, the quadratic law splits the entire star up until 14 shells at different radii on the star reflected by the 14 cases rather than just breaking a transit up into ingress/egress, full eclipse, and no eclipse as the linear law and small planet approximation do (see Equation 2.1). Each case corresponds to a different distance from the center of the star, so the form of the limb darkening varies depending on how close the planet is to the edge. Unlike the small planet approximation (see Section 2.1.2), the quadratic treatment does not assume that limb darkening is uniform under the entire area blocked by the transiting planet. This form is therefore much more accurate for large planets ($p \geq 0.10$). A sample light curve generated using the quadratic treatment of limb darkening is given in Figure 2.6.

Table 2.2: Quadratic Limb Darkening

Case	p	z	λ_d	$\eta_d(z)$
1	$(0,\infty)$	$[1+p,\infty]$	0	0
2	$(0,\infty)$	$(\frac{1}{2}+\lvert p-\frac{1}{2}\rvert, 1+p)$	λ_1	η_1
3	$(0,\frac{1}{2})$	$(p,1-p)$	λ_2	η_2
4	$(0,\frac{1}{2})$	$1-p$	λ_5	η_2
5	$(0,\frac{1}{2})$	p	λ_4	η_2
6	$\frac{1}{2}$	$\frac{1}{2}$	$\frac{1}{3}-\frac{4}{9}\pi$	$\frac{3}{32}$
7	$(\frac{1}{2},\infty)$	p	λ_3	η_1
8	$(\frac{1}{2},\infty)$	$[\lvert 1-p\rvert, p)$	λ_1	η_1
9	$(0,1)$	$(0,\frac{1}{2}-\lvert p-\frac{1}{2}\rvert)$	λ_2	η_2
10	$(0,1)$	0	λ_6	η_2
11	$(1,\infty)$	$[0,p-1)$	1	1
12	$(0,\frac{1}{2})$	$\lvert p+z-1\rvert \le .0001$	λ_5	η_2
13	$(\frac{1}{2},\infty)$	$\lvert p+z-1\rvert \le .0001$	λ_5	η_1
14	$(0,\infty)$	$[0,p)$	$\lambda_d+\frac{2}{3}$	η_d

A revised table of the values given in Table 1 of Mandel & Agol (2002). Cases 12 and 13 represent the new case discussed in Section 2.1.4.

$$\lambda_1 = \frac{1}{9\pi\sqrt{pz}}\left[[(1-b)(2b+a-3) - 3q(b-2)K(k) + 4pz(z^2+7p^2-4)E(k) - 3\frac{q}{a}\Pi(\frac{a-1}{a},k)\right] \tag{2.6}$$

$$\lambda_2 = \frac{2}{9\pi\sqrt{1-a}}\left[(1-5z^2+p^2+q^2)K(k^{-1}) + (1-a)(z^2+7p^2-4)E(k^{-1}) - 3\frac{q}{a}\Pi(\frac{1-a}{a},k)\right] \tag{2.7}$$

$$\lambda_3 = \frac{1}{3} + \frac{16p}{9\pi}(2p^2-1)E(\frac{1}{2p}) - \frac{(1-4p^2)(3-8p^2)}{9\pi p}K(\frac{1}{2p}) \tag{2.8}$$

$$\lambda_4 = \frac{1}{3} + \frac{2}{9\pi}[4(2p^2-1)E(2p) + (1-4p^2)K(2p) \tag{2.9}$$

$$\lambda_5 = \frac{2}{2\pi}\cos^{-1}(1-2p) - \frac{4}{9\pi}(3+2p+-8p^2)\sqrt{p-p^2} \tag{2.10}$$

$$\lambda_6 = -\frac{2}{3}(1-p^2)^{\frac{3}{2}} \tag{2.11}$$

$$\eta_1 = (2\pi)^{-1}[\kappa_1 + 2\eta_2\kappa_0 - \frac{1}{4}(1+5p^2+z^2)\sqrt{(1-a)(b-1)}] \tag{2.12}$$

$$\eta_2 = \frac{p^2}{2}(p^2+2z^2) \tag{2.13}$$

$$k = [(1-a)/(4zp)]^{\frac{1}{2}}] \tag{2.14}$$

$$q = p^2 - z^2 \tag{2.15}$$

Expressions for κ_1 and κ_0 are given in Equations 2.2 and 2.3. $E(k)$ is the complete elliptic integral of the first kind, $K(k)$ is the complete elliptic integral of the second kind, and $\Pi(n,k)$ is the complete elliptic integral of the third kind. These elliptic integrals arise in the quadratic form of the limb darkening law because the quadratic law is actually a specific form of the nonlinear law given in Mandel & Agol (2002). The linear law reduces to the quadratic law in the case when the nonlinear limb darkening coefficients (a_1, a_2, a_3, and a_4) are $a_1 = a_3 = 0$ and $a_2 = \mu_1 + 2\mu_2$ and $a_4 = -\mu_2$ where μ_1 and μ_2 are the quadratic limb darkening coefficients. In this limit the hypergeometric functions in the nonlinear form (see Section 3 of Mandel & Agol (2002)) reduce to this set of elliptic integrals. This is useful for calculations since elliptic integrals are more easily calculated than hypergeometric functions.

Elliptic Integrals

For programming purposes, it is necessary to find some useful approximation of the complete elliptic integrals. It is possible to represent $E(k)$ and $K(k)$ as polynomial approximations known as Hastings approximations (Hastings 1955). Since this is a polynomial approximation, all the terms are simply coefficients except for the term k which is the input value of the elliptic integrals $E(k)$ and $K(k)$. Equation 2.14 gives a definition for k. The Hastings approximations are as follows:

$$X = [a_0 + (1-k^2)(a_1 + (1-k^2)(a_3 + (1-k^2)a_4))] \tag{2.16}$$

$$Y = [(b_0 + (1-k^2)(b_1 + (1-k^2)(b_2 + (1-k^2)(b_3 + (1-k^2))b_4)))) \ln(1-k^2)] \tag{2.17}$$

$$K(k) = X - Y \tag{2.18}$$

$a_0 = 1.38629436112$ $a_1 = 0.09666344259$ $a_2 = 0.03590092383$
$a_3 = 0.03742563713$ $a_4 = 0.01451196212$
$b_0 = 0.5$ $b_1 = 0.12498593597$ $b_2 = 0.06880248576$
$b_3 = 0.03328355346$ $b_4 = 0.00441787012$

$$U = 1 + (1-k^2)(c_1 + (1-k^2)(c_2 + (1-k^2)(c_3 + (1-k^2)c_4))) \tag{2.19}$$

$$V = (1-k^2)(d_1 + (1-k^2)(d_2 + (1-k^2)(d_3 + (1-k^2)d_4))) \ln(1/(1-k^2)) \tag{2.20}$$

$$E(k) = U + V \tag{2.21}$$

$c_1 = 0.4432514146$ $c_2 = 0.06260601220$ $c_3 = 0.04757383546$ $c_4 = 0.01736506451$
$d_1 = 0.24998368310$ $d_2 = 0.09200180037$ $d_3 = 0.04069697526$ $d_4 = 0.00526449639$

It is also useful to note that all elliptic integrals can be reduced to a set of elliptic integrals known as the Carlson Symmetric forms (Mandel & Agol 2002). The complete elliptic integrals can be expressed as Carlson elliptic integrals as

follows:

$$K(k) = R_j(0, 1-k^2, 1) \tag{2.22}$$

$$E(k) = R_f(0, 1-k^2, 1) - \frac{1}{3}R_d(0, 1-k^2, 1) \tag{2.23}$$

$$\Pi(n,k) = R_f(0, 1-k^2, 1) + \frac{1}{3}nR_j(0, 1-k^2, 1, 1-n) \tag{2.24}$$

$K(k)$ and $E(k)$ can thus most easily be calculated using a Hastings approximation, but $\Pi(n,k)$ requires calculating R_j and R_f. This can be done using a numerical recipes routine (Press et al. 2007).

2.1.4 A New Case in the Quadratic Limb Darkening Law

Without adding an additional case to the 11 outlined in Mandel & Agol (2002), the quadratic limb-darkened curves will have a few points with undefined values. These points correspond to $z = 1 - p$ or $z = p$. Such undefined points do not happen for all p values, only for $0.1 < p < 1.0$. Though one missing point may not be obvious just looking at the light curve, these undefined points can potentially cause fatal errors when using these model light curves to fit actual data. Therefore, it is essential to add an additional case that takes care of many of the undefined points.

Most of the undefined data points can be corrected by adding a new case to the 11 listed by Mandel & Agol (2002). In Mandel & Agol (2002), case 8 is used for $z = 1 - p$ where $p > 0.5$ and case 4 is used for $z = 1 - p$ where $p < 0.5$. Instead, use the case where $\mid p + z - 1 \mid \leq 0.0001$ (this is where $1 - p$ approaches z). In this case, $\lambda_d = \lambda_5$. The cases from Mandel & Agol (2002) can still be used to determine η_d. These corrections are reflected in cases 12 and 13 in Table 2.2.

While this approach does substantially decrease the number of problematic

points, for certain input values of p there may be undefined points, though these occur rarely. These are usually caused by an error in the Numerical Recipes routine used in computing the elliptic integrals, but they may also occasionally be due to a problem when computing λ_d. This problem remains unresolved, but when executing the program an error message will print to the screen notifying the user if there are any undefined points and at what z values these holes occur. If there is an error computing the elliptic integrals, an error message may come up saying "wrong size in rj, "wrong size in rc," "wrong size in rf," "invalid arguments in rf," "invalid arguments in rc," or "invalid arguments in rj." Note that this error message may come up while AMOEBA is running and will print to the screen. Generally this is not a problem, and only indicates that AMOEBA has strayed outside values for which the elliptic integrals can be computed. AMOEBA should move away from these values and continue running, though it is possible that AMOEBA could get stuck at values where these errors occur and crash. AMOEBA will be discussed in detail in Section 2.2.2.

2.1.5 Generating Model Light Curves

For these three treatments of limb darkening, the uniform source, the small planet approximation, and the quadratic law, I have written programs capable of generating a model light curve given specific model input. For the uniform source, due to its relative simplicity, the only necessary input required is p, the ratio of R_p to R_*. As discussed, this light curve gives only a sense of the depth of eclipse. The overall shape of the curve is inaccurate and would not accurately fit parameters to actual data.

Because the small planet approximation and the quadratic limb darkening

law take in to account the limb darkening, both require the input of stellar limb darkening coefficients in addition to p. These can be obtained from models such as Claret (2000).

Up until now, the limb darkening laws appear to take into account only p and the limb darkening coefficients, but transit data is also useful for determining the inclination of the orbit, the center of transit, and the ratio of the semimajor axis to the stellar radius. In order to fit these additional parameters it is necessary to convert impact parameter (z) to time (t). The limb darkening is computed using impact parameter (z) in Mandel & Agol (2002), and a light curve can be produced that relates the normalized flux of the system to the impact parameter. This impact parameter can be converted to time using the following equation (Mandel & Agol 2002):

$$z = a_p/r_*[(\sin(\omega t)^2 + (\cos(i)\cos(\omega t)^2]^{1/2} \tag{2.25}$$

where a_p is the semimajor axis at periastron, r_* is the stellar radius, ω is the orbital frequency, i is the inclination, z is impact parameter, and t is the time from center of transit. This conversion has been used to produce Figure 2.5, for example.

The most accurate of these three limb darkening laws, and the law that is valid over the largest range of radii ratios, is the quadratic law. See Section 2.1.3 for a more detailed explanation of the advantages of the quadratic limb darkening treatment. Because of these advantages, this is the law that I have chosen to use to fit actual light curve data in the sections that follow.

2.2 Fitting the Model

With programs that will generate model transit light curves in hand, it is possible to use these models to fit data from actual transit light curves in order to obtain their system parameters. To do this I used the program I wrote to produce model light curves using quadratic limb darkening as well as an IDL routine called AMOEBA to implement chi-squared minimization.

2.2.1 Downhill Simplex Method

In order to fit a model light curve to an actual transit light curve it is necessary to find some routine that can fit the best possible model to the data by minimizing the deviation of the model fit from the data. For this particular task, this method needs to be able to perform a multidimensional fit capable of fitting at least four free parameters (inclination [i], stellar radius [R_*], planetary radius [R_p], transit center time [t_c]) or more, as it is also possible to fit two limb darkening coefficients (μ_1, μ_2) and to simultaneously fit several transit curves which necessitates fitting multiple t_c simultaneously. To do this I have used a technique known as the downhill simplex method in multiple dimensions (Press et al. 2007). The goal of this method is to find the minimum of a function with more than one independent variable.

A simplex is an N-dimensional geometric figure with $N+1$ vertices where N is the number of independent variables of the function that needs to be minimized. This simplex encloses some finite N-dimensional volume. In order to begin the multidimensional fit it is necessary to define some initial simplex, that is, initial guesses for each of the free parameters. The downhill simplex method then begins

a series of steps pulling and stretching the simplex (that is, taking a series of steps away from the values of initial guesses) to hone in on a best fit point. Because this fit is multidimensional, it is impossible to simply bracket the best fit of one variable in order to define when the fit is good enough. Instead it is necessary to define a fractional tolerance. The final step of the simplex method must decrease the function value by an amount fractionally smaller than this defined fractional tolerance in order for the fitting process to be complete (Press et al. 2007).

2.2.2 AMOEBA

There is an IDL routine that utilizes this downhill simplex method called AMOEBA. In order for AMOEBA to work, it is first necessary to provide it with a function to be minimized. This can be any statistic that describes the quality of the fit to the data. In this case, I have chosen to use chi-squared minimization. AMOEBA, then, is minimizing the χ^2 function (Bevington & Robinson 1992)

$$\chi^2 = \sum_{j=1}^{n} \frac{[h(x_j) - NP(x_j)]^2}{\sigma_j(h)^2} \tag{2.26}$$

where $h(x)$ represents the distribution of measurements, N is the total number of measurements, $P(x)$ is the expected outcome, and σ is is the standard deviation of the observations. In this particular case, each $h(x_j)$ represents a point on the observed light curve, each $P(x_j)$ represents the corresponding point on the model light curve, N represents the total number of data points in the light curve, and σ is a measurement of the error on each observation. It is easy to calculate σ from the errors in the observations using the equation (Bevington & Robinson 1992):

$$\sigma = (\frac{1}{N}\sum_{j=1}^{n}\frac{1}{error^2})^{-1} \tag{2.27}$$

AMOEBA also requires as input the fractional tolerance required for each free parameter in order for the fit to be considered good enough. This fractional tolerance can theoretically be very small, even of the order of machine precision, but the lower the fractional tolerance the longer the required computing time (Press et al. 2007). Setting the ideal fractional tolerance for a given minimization function is largely a matter of individual discretion, balancing the desire for the best possible fit with the necessity of limiting computation time. For this light curve fit, a fractional tolerance of about 10^{-7} is sufficient to accomplish the necessary accuracy. A fractional tolerance of the order 10^{-6} results in a substantially higher minimum χ^2. A fractional tolerance of 10^{-8} does not significantly change the minimum χ^2 value but does require significantly longer computing time.

The only other required input into AMOEBA is a set of initial guesses for all the free parameters, guesses that define AMOEBA's initial simplex, and an array of bracketing values that describe how much each parameter should be allowed to vary. AMOEBA starts by computing the chi-squared value for the light curve defined by these initial values. It then repeats this calculation over and over, stepping slightly away from these starting values with each iteration and honing in on a minimum χ^2 value.

This process works well. There are, however, a few ways in which AMOEBA is not perfectly suited to this type of fitting. The most important is that the input parameters which define how far AMOEBA may stray from the initial guesses is not a hard limit. In many cases, AMOEBA may override these limits if the computation indicates the function minimum may exist beyond these boundaries.

This is unacceptable in the case that these limits are defined by physical or mathematical laws. These limits are as follows:

1) The limb darkening coefficients in the quadratic law are subject to some constraints, as the quadratic law is actually a reduction of the nonlinear law given in Mandel & Agol (2002), and the nonlinear law only reduces to this form if the 4 nonlinear limb darkening coefficients are taken to be $c_1 = c_3 = 0$ and $c_2 = \mu_1 + 2\mu_2$ and $c_4 = -\mu_2$ and $\mu_1 + \mu_2 < 1$ where μ_1 and μ_2 are the quadratic limb darkening coefficients and must be either determined from a model or left as a free parameter that AMOEBA will fit. In the case that these are left as free parameters, it becomes necessary to enforce the limit that $\mu_1 + \mu_2 < 1$.

Similarly, if $\mu_1 + \mu_2 < 0$, the shape of the light curve will bend upwards in the center of the curve instead of downward (See Figure 2.7). This is not a physically realistic model, and limb darkening values that yield such a light curve should never produce the best fit. However, because the limb darkening coefficients are often not well constrained by the light curve, in some situations AMOEBA seems to get stuck using such negative limb darkening values and begins to try to find the minimum χ^2 for a function of this strange shape. To avoid this problem altogether it is useful to impose this hard limit on the limb darkening coefficients as well.

2) R_* and R_p cannot be negative. Obviously this is a nonphysical situation that should never be fitted, but it is possible for AMOEBA to go in the wrong direction, get stuck, and return such nonsense values. To protect against this, it is again desirable to set the hard limit that $R_* > 0$ and $R_p > 0$.

3) If inclination is allowed to vary freely, AMOEBA is equally likely to return a value above 90° as it is to return one between 0 and 90°. This does not affect the computation, but for simplicity we can define a hard limit to inclination such that $0 \leq i \leq 90°$.

In order to implement these hard limits we simply have AMOEBA return an artificially high χ^2 value any time it attempts to stray outside these bounds.

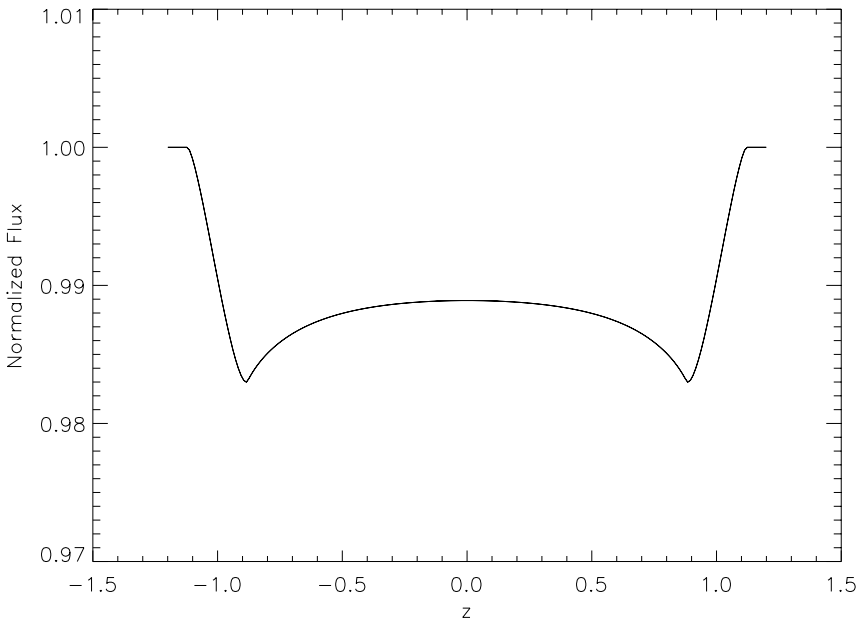

Figure 2.7: Lightcurve with $\mu_1 + \mu_2 < 0$

2.2.3 Limb Darkening Coefficients

One difficulty in fitting a light curve is how to deal with the stellar limb darkening. Theoretically it is possible to set the limb darkening coefficients and fit them to the light curve. The problem is that these coefficients are only weakly constrained by the shape and depth of a light curve, and thus it is possible for them to vary significantly. This greatly increases the error on the results of a fit. Different groups have treated the limb darkening coefficients differently. Some

have attempted to fit the limb darkening (Holman et al. 2006; Southworth et al. 2007). Others have opted instead to fix the limb darkening parameters to model values (Charbonneau et al. 2002; Bakos et al. 2009) Some groups have tried both techniques and compared the results (Holman et al. 2007).

I have made use of both methods, and the specific results are detailed in Chapter 3. Table 3.1 gives a summary of these results . The conclusion reached in this thesis is that the quality of the data required to actually obtain good fits for the limb darkening parameters is extremely high, and even then the coefficients are fairly weakly constrained. Attempts to derive the limb darkening purely by fitting them to a light curve are optimistic, even with high quality data, and especially for transits obtained with Wesleyan's 24" telescope, it is impossible to obtain a light curve of high enough precision to accurately fit these. Nevertheless, the fitting program is capable of using either option, either fitting the limb darkening coefficients or using fixed model values.

Chapter 3

Results of Light Curve Analysis

Fitting program in hand, I first set out to show that the results from my program were consistent with those obtained by other groups. The first test I ran was running my fitting program on data obtained from the Holman et al. (2007) paper analysis of the transit light curves of TrES-2. After confirming that my results agreed with results in the literature, I was able to start fitting data acquired at Wesleyan.

3.0.4 Testing the Fit

Holman et al. (2007) set out to analyze the transit light curves of TrES-2. TrES-2 lends itself well to study because it is large and nearby, with a fairly high $\frac{R_p}{R_*}$ and bright apparent magnitude ($m_v = 11.41$), making the host star easily visible with a small ground based telescope and the transit light curve fairly deep (the depth of the light curve is determined by p^2). For a full summary of the system parameters of TrES-2 see Tables 4.3 and 4.4. Holman et al. (2007) analyze the data from three separate transits of TrES-2 and provide all their data online, so this data was easy to obtain and run through my fitting program. Holman et al. (2007) use a similar fitting routine that also uses AMOEBA to minimize χ^2, so the results should agree well. It is thus a good test of the accuracy of my fits. A comparison of the system parameters determined by Holman, by me using

Table 3.1: System Parameters of TrES-2 using Three Different Fits

Parameter	a	b	c
R_* ($R_\odot$)	1.003 ± 0.017	1.004 ± 0.021	0.9800 ± 0.036
R_p ($R_\odot$)	1.222 ± 0.028	1.225 ± 0.026	1.212 ± 0.038
p	0.1253 ± 0.0010	0.1254 ± 0.0047	0.1271 ± 0.0141
i (deg.)	83.57 ± 0.14	83.56 ± 0.01	$83.97 \pm .23$
μ_1	0.22	0.22	0.50 ± 0.21
μ_2	0.32	0.32	0.41 ± 0.12
$t_c(1)$ $(HJD - 2,450,000)$	$3,989.75286 \pm 0.00029$	$3,989.7529 \pm 0.00012$	$3,989.7529 \pm 0.00012$
$t_c(2)$ $(HJD - 2,450,000)$	$3,994.69393 \pm 0.00031$	$3,994.6939 \pm 0.00024$	$3,994.6939 \pm 0.00022$
$t_c(3)$ $(HJD - 2,450,000)$	$4,041.63579 \pm 0.00030$	$4,041.6360 \pm 0.00022$	$4,041.6360 \pm 0.00022$

The values in column a are obtained in Holman et al. (2007) using fixed limb darkening coefficients(μ_1 and μ_2), as well as a fixed orbital period of 2.47063 days and fixed M_* at .98 $M_\odot$ adopted from Sozzetti et al. (2007).
The values in column b are the output of my fitting program assuming fixed limb darkening coefficients. In this case I have fixed the limb darkening coefficients to be the same used in Holman et al. (2007). The fit also adopts fixed values of $a_p = .03556$ AU and the same period as Holman et al. (2007), P= 2.47063 days.
The values in column c are the output of my fitting program with fitted limb darkening coefficients. The same values for a_p and P from the column b fit are used.

fixed limb darkening coefficients, and by me while fitting the limb darkening is given in Table 3.1.

The results from the fixed limb darkening fits are very similar to the results obtained in Holman et al. (2007) to well within errors (see Table 3.1). It should be noted that there are a few differences in the fitting procedure adopted by Holman et al. (2007) as opposed to my procedure. They used a fixed value of $M_* + M_p$ and use this to determine the semimajor axis (a_p), whereas I just adopted a semimajor axis determined from radial velocity measurements (Daemgen et al. 2009). They used an iterative fitting process in which they first assumed a value M_*, then fitted the light curves for the quantity $\frac{R_*}{a_p}$ because this quantity is independent of M_* (both R_* and a_p are proportional to $M_*^{1/3}$). They then used the quantity $\frac{R_*}{a_p}$ to refine the estimate for M_* through Kepler's third law. They used a similar iterative process to refine their estimates for limb darkening coefficients as well,

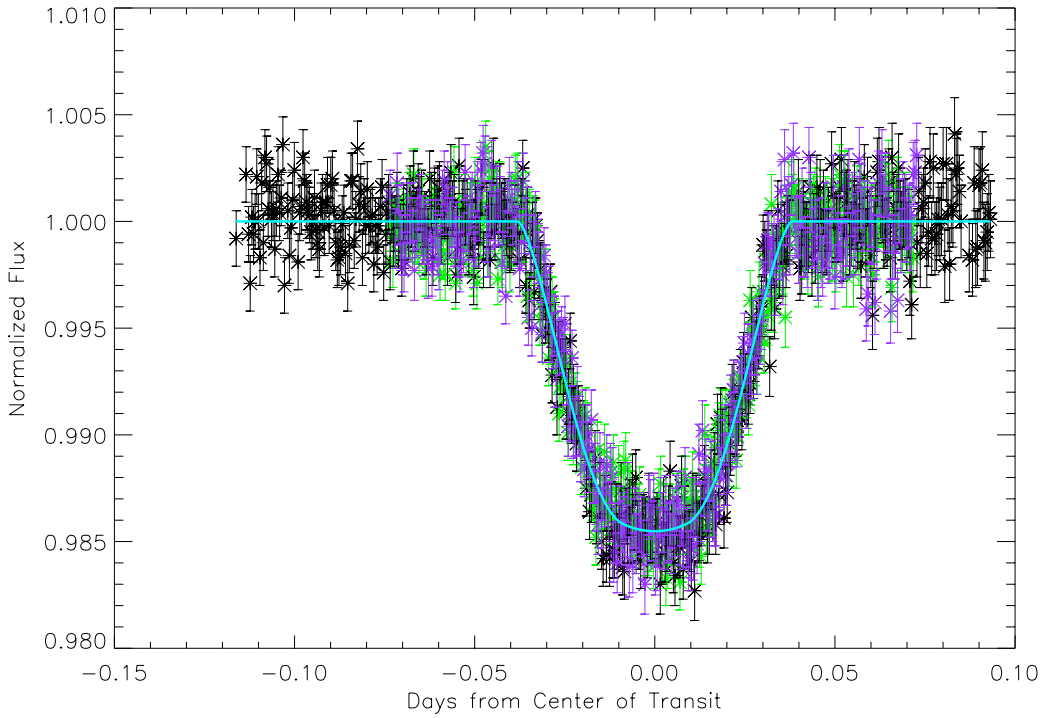

Figure 3.1: 3 different transit light curves for TrES-2 taken from Holman et al. (2007) and fit using my program. The light curve in black is the transit from the night of September 11, 2006; the green light curve is from September 16, 2006 and the purple light curve is from November 2, 2006. The fit from my program is overlaid in light blue.

passing values through several iterations before picking fixed values with which to do their final fit.

It should also be noted that Holman et al. (2007) use AMOEBA to fit the out of transit flux as a function of airmass, something that we do not do (Holman et al. 2007). Though it does not affect the results of this comparison since I took their determined values for normalized flux directly from the Holman et al. (2007) paper, it may affect the results for light curves obtained and reduced at VVO.

3.0.5 Error Determinations

Errors on each parameter were determined using a one dimensional confidence limit. In essence, I held all but one parameter fixed at their best fit values and calculated how the χ^2 value changed when varying just this one parameter. I then converted the resulting distribution of χ^2 values to a 68 percent confidence interval using the IDL function `chisqr_cvf` to find the 1σ errors. This function returns the deviation from the minimum χ^2 value that corresponds to a given standard deviation given the number of degrees of freedom. For example, if I froze every parameter except for R_*, `chisqr_cvf(1-.683, 1)` would return the bounds on a 68 percent confidence interval given one degree of freedom. If the minimum χ^2 value was 1, and this function returned a value of 2, then any value R_* that resulted in a χ^2 value between 1 and 3 would be within this 68 confidence interval. Finding the R_* values within these bounds, then, provides the 1σ uncertainties. These uncertainties are listed in Table 3.2.

These results do not factor in the errors introduced by the semi-major axis (a_p) and orbital frequency (ω), values we fixed in the fitting process. The errors in the orbital frequency are so small that they do not significantly impact the fit results,

Table 3.2: Error From χ^2 Confidence Interval

Parameter	Fixed Limb Darkening Best Fit Value	σ
R_s	1.0038	$\pm$0.0010
R_p	1.2248	$\pm$0.0036
i	83.5622	$\pm$.01
p	0.12542	0.0047
t_1	3,989.75289	$\pm$0.00012
t_2	3,994.69394	$\pm$0.00024
t_3	4,041.63597	$\pm$0.00022
	Fit Limb Darkening	
R_s	0.9800	$\pm$0.0010
R_p	1.2121	$\pm$0.0036
i	83.9674	$\pm$0.006
p	0.12714	0.0141
t_1	3,989.75290	$\pm$0.00012
t_2	3,994.69394	$\pm$0.00022
t_3	4,041.63597	$\pm$0.00022
μ_1	0.50	$\pm$0.01253
μ_2	0.41	$\pm$0.0183

a conclusion reached by Holman et al. (2007) as well. However, the errors on a_p are large enough to have a significant impact on the uncertainties, though due to the complexity of the limb darkening equations, it is not immediately obvious how this error will affect the other parameters.

To provide rigorous uncertainties based on the error in a_p would require a full Markov Chain Monte Carlo (MCMC). I have not yet done this complete error analysis. However, to gauge the magnitude of the impact of this error on the overall uncertainties, I refit the light curves using values of a_p that deviate from the best estimate by 1σ. I used the value $a_p = .03556 \pm .00075$ from Daemgen et al. (2009). The results from refitting the light curves using $a_p + \sigma$ and $a_p - \sigma$ using fixed limb darkening coefficients are given in Table 3.3. The results from refitting

the light curves using fitted limb darkening coefficients are given in Table 3.4. The errors given in Table 3.1 were determined by adding in quadrature the error in a_p (given in Tables 3.3 and 3.4) and the errors obtained from the confidence interval method outlined above (given in Table 3.2). It is important to note that the dominant source of the error in R_* and R_p is from the uncertainty in the a_p measurement, but the error in all other quantities is dominated by the error determined from the χ^2 confidence interval. Though this is not a thorough error analysis employing a MCMC–and such an analysis should be done in the future–these estimates are helpful in gauging the overall magnitudes and sources of error for each parameter. It should also be noted that, though the fitting procedures used by Holman et al. (2007) are similar to mine and my results agree quite well, Holman et al. (2007) do fit a_p/R_* and R_p/R_* rather than R_* and R_p. They also adopt a value for M_* rather than a value for a_p as I do. Thus, their errors may be expected to differ somewhat from mine due to this alternative approach.

Table 3.3: Error Analysis for Fixed Limb Darkening

Parameter	a_p	$a_p + \sigma$	$a_p - \sigma$
R_s	1.0039	+0.0212	−0.0212
R_p	1.2249	+0.0258	−0.0260
i	83.5623	1.72e-4	9.38e-6
p	0.12542	2.42e-6	−5.75e-6
t_1	3,989.75290	6.2e-7	1.02e-6
t_2	3,994.69394	1.57e-7	−2.38e-6
t_3	4,041.63597	1.43e-6	3.3e-6

A rough analysis of the error introduced to the best fit parameters because of the error in a_p is shown above. The first column lists the free parameters. The first second lists the best fit value calculated by our fitting program. The third column gives the change in this value when the value assume for a_p is raised by 1σ. The last column gives the change in the best fit value when the value of a_p is lowered by 1σ. For this fit the limb darkening coefficients have been fixed at $\mu_1 = 0.22$ and $\mu_2 = 0.32$, the values adopted by Holman et al. (2007). In this case, $a_p = 0.03556 \pm .00075$, values adopted from Daemgen et al. (2009), so $a_p + \sigma = 0.03631$ and $a_p - \sigma = 0.03481$.

Table 3.4: Error analysis for Fitted Limb Darkening

Parameter	a_p	$a_p + \sigma$	$a_p - \sigma$
R_s	0.97998	0.0448	−0.0262
R_p	1.2121	0.0358	−0.0413
i	83.97	-0.3619	0.09949
t_1	3,989.75290	3.4e-5	−2.0e-6
t_2	3,994.69394	1.9e-5	9.3e-7
t_3	4,041.63597	−1.0e-7	−2.0e-7
μ_1	0.50	−0.42	+0.01
μ_2	0.41	+0.17	−0.08

This is a similar table to Table 3.3. The a_p values are the same. The only difference is that for this fit the limb darkening coefficients were left as free parameters. Note that the error estimates are similar to those for the parameters given in Table 3.3, but that the error in the limb darkening coefficients is quite large.

Chapter 4

Observations at Van Vleck

The final stage of this project was to set up an observing program on Wesleyan's 24" telescope and obtain observations of a transiting exoplanet that could then be analyzed using my model. Due to a combination of bad weather, a technical malfunction of the CCD that resulted in a 3-month observing hiatus, and a wasp infestation in the warm room, I was only able to obtain a light curve for one transit of the exoplanet TrES-2. One light curve is not a large enough data set to obtain a very precise fit, but I was able to experiment with some new observing techniques, perfect the set of programs used to reduce the data, and perform a preliminary fit on the light curve. Though more data would be desirable in order to obtain a more accurate fit using my programs, this transit confirms that it is possible to use the telescope at Van Vleck Observatory to procure meaningful transit data.

4.1 Selecting Targets

The original aim of this project was to select two transiting exoplanet targets. One would be a well-studied planetary system with properties making it fairly easy to observe. This would be a target that was relatively nearby and bright, but also one with a deep light curve. The depth of the light curve is determined by the R_p to R_* ratio (called p), so picking a system with a large p value was impor-

tant. We were confident that observations of a planet meeting these requirements could be obtained using Wesleyan's telescope. Additionally, by picking a well-studied planet, our results for the best fit values of the system parameters could be compared to results in the literature to test the accuracy of our observation, reduction, and analysis procedures.

The other target ideally would have been a planet that pushed the limits of our observational powers. This could be a fainter, more distant system and/or a system with a smaller p value. Most importantly, though, it would be a planet that had not been previously well investigated so that observations at VVO could potentially constrain the system parameters further. Unfortunately, bad weather and technical malfunctions prevented us from obtaining any observations of such a lesser-known system, but it remains a promising idea for a future project.

Initially the pool of candidate targets consisted of all known transiting exoplanets listed in the Extrasolar Planets Encyclopedia as of September 2009, about 60 candidates in total. I then eliminated any transiting planets that had fewer than nine transits observable from VVO between September 2009 and December 2009, the period during which I intended to gather the bulk of my data. This list was further narrowed to exclude Corot-7b, a very small planet with a very small p value that we would be unable to detect from VVO. This left the 15 potential target candidates listed in Table 4.1. Of these potential targets a few attributes stuck out. First, it was desirable to select a target with $p \geq 0.10$ in order to test the quadratic limb-darkening law (detailed in Section 2.1.3), since with a smaller p the small planet approximation limb darkening law is sufficient (see Section 2.1.2). Secondly, we wished to first select a well-observed, large, bright system for our first set of observations so we could obtain high quality transit data and test our results by comparing them to results in the literature. This necessitated picking

an easily observable star with a bright apparent magnitude, a large p value, and several high quality transits (transits near the zenith for which the star is visible for the duration of the entire transit), as well as a system that had been studied in a number of other publications. Given this criteria, TrES-2 stuck out as a desirable target, as it has a large p value ($p = .125$ according to Holman et al. (2007), $p = .131$ according to The Exoplanet Encyclopedia (Schneider 2010)) necessitating the use of the quadratic law, a fairly bright host star (V-band apparent magnitude of 11.42), with 9 observable transits of which 6 could be called high quality (airmass above 2 for the entire duration of the transit). A full summary of the stellar and planetary parameters of TrES-2 are given in Table 4.3 and Table 4.4 and a full transit schedule for the 2009-2010 observing season is given in Table 4.2. TrES-2 is also the subject of 45 published papers, including a Transit Light Curve Project paper (Holman et al. 2007, the paper to which we compared our results in Chapter 3 to test our fitting program) that has made its data publicly available and uses a similar light curve fitting scheme to ours. Notably, TrES-2 is in the field of *Kepler* (Holman et al. 2007).

4.2 Observations of TrES-2

The main challenge of observing a transit event is that the amount of light blocked by the transiting planet is quite small–typically around a 1-2 percent decrease in the normalized flux. A typical transit lasts for a few hours (TrES-2 has a 90 minute transit) and assembling an accurate light curve requires minimizing any other sources of brightness variation over the total period of the transit. This requires carefully correcting for changes in visiblity and changes in airmass, but it also means that even pixel to pixel sensitivity variations in the CCD can be

Table 4.1: Characteristics of Transiting ExoplanetTarget Candidates Observable from Van Vleck Observatory

Planet	Year of Discovery	Observable Transits[1]	p^2	V-band Mag. [3]	Publications
HAT-P-7	2008	10	0.079	10.5	14
HAT-P-13	2009	10	0.084	10.6	2
XO-4	2008	10	0.089	10.7	9
XO-3	2007	14	0.091	9.8	28
HAT-P-8	2008	9	0.098	10.2	2
WASP-1	2006	15	0.101	11.8	33
WASP-3	2007	9	0.103	10.6	17
XO-2	2007	12	0.104	11.2	26
HAT-P-1	2006	9	0.113	10.4	43
WASP-12	2008	30	0.117	11.69	9
TrES-2	**2006**	**9**	**0.131**	**11.4**	**45**
WASP-11/HAT-P-10	2008	12	0.133	11.9	7
Corot-1-b	2007	13	0.138	13.6	20
WASP-10	2008	10	0.142	12.7	13
TrES-3	2007	9	0.164	12.4	33

[1]number of transits observable from VVO between September 1, 2009 and December 31st, 2009.
[2]p, the ratio between R_p and R_*.
[3]apparent V-band magnitude of the planet's host star.
Note– all these numbers were taken from the Extrasolar Planets Encylopedia at http://www.exoplanet.eu. This information was current as of September 5, 2009, the time of candidate selection.

problematic in assembling an accurate transit light curve if the star moves all over the field of view. To minimize these effects, it is desirable to keep the star on the same set of pixels for the entire duration of a transit, a task made difficult at VVO because there is no autoguiding.

We implemented a few new observing techniques to minimize the impact of the star wandering in the CCD window. First, we intentionally defocused the telescope to spread the starlight over more pixels, keeping the focus just good enough to prevent the stars from taking on a doughnut appearance. Second, we monitored the location of the star throughout the 90 minute transit, occasionally stopping and recentering the star as needed to keep the star within about 10 pixels of its starting location. Though this technique is not extremely precise, it cuts down substantially on how far the star wanders from center (see Figure 4.1–4.2).

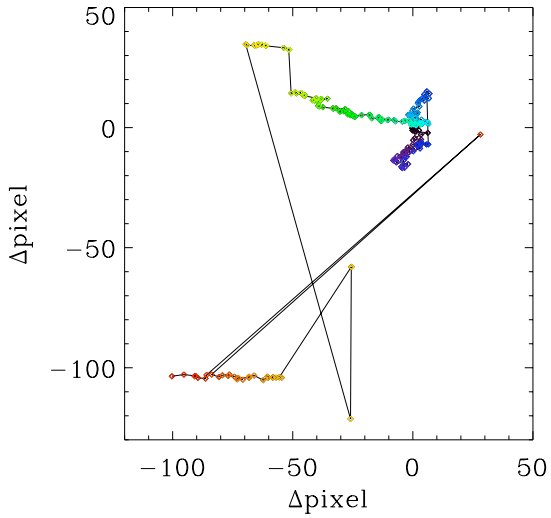

Figure 4.1: This plot shows the movement of the centroid value of XO-5 over time. The colors represent time. Purple is earliest, red is latest. The x-axis shows the offset in the x direction from the starting centroid value; the y-axis shows the offset in the y direction. These observations were obtained at VVO on the night of February 24, 2009 without using the defocusing or recentering technique.

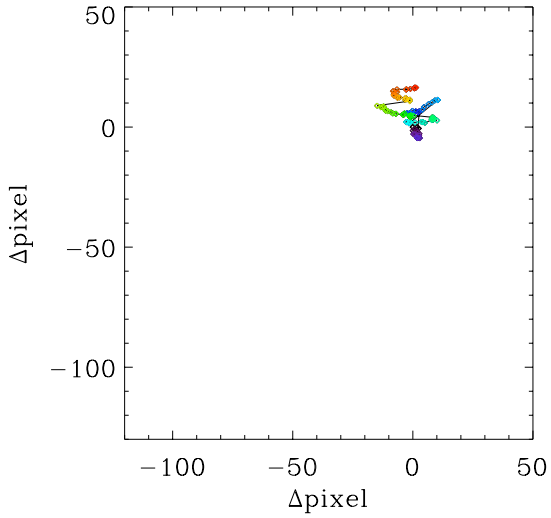

Figure 4.2: This is the same plot as Figure 4.1 for observations of TrES-2 obtained on September 21, 2009 at VVO using the defocusing and recentering technique. Note that the change in centroid value is much smaller than in Figure 4.1.

Observations of TrES-2 were taken on the night of September 21, 2009 using Wesleyan's 24" telescope. Though this is the only transit observed for this thesis, for a full list of the predicted transit times of TrES-2 during the 2009-2010 academic year see Table 4.2. For the September 21st transit, the sky was clear, the transit occured at low airmass, and the entirety of the transit was visible. Observations were made by taking repeated 60 second exposures in the I-filter for the entire duration of the transit. It is also necessary to observe the system for some time before first contact and after fourth contact in order to ascertain the out-of-transit flux. These observations extend from 30 minutes before the predicted transit start time to 15 minutes after the predicted end. For future observations, taking more observations before and after the transit would be advisable in order to better fit the out of transit flux. The transit data was reduced using the IRAF script `reduceI`, which performs the flat fielding and dark and bias subtraction. Several IDL routines were used to determine the best aperture size to measure the flux and the flux was calibrated using 5 comparison stars in the field of TrES-2. The resulting light curve is shown in Figure 4.3.

Table 4.2: 2009-2010 Observing Season TrES-2 Transit Schedule

Start			**Center**			**End**			
Date	Time	Airmass	Date	Time	Airmass	Date	Time	Airmass	Notes
Sept. 21	9:30 PM	1.01	Sept. 21	10:15 PM	1.02	Sept. 21	11:00 PM	1.04	Observed
Sept. 26	8:02 PM	1.03	Sept. 26	8:47 PM	1.01	Sept. 26	9:32 PM	1.01	Bad Weather
Oct. 1	6:38 PM	1.01	Oct. 1	7:23 PM	1.01	Oct. 1	8:08 PM	1.02	Wasps
Oct. 28	10:53 PM	1.70	Oct. 28	11:38 PM	2.06	Oct. 29	12:23 AM	2.56	Bad Weather
Nov. 2	9:28 PM	1.39	Nov. 2	10:13 PM	1.59	Nov. 2	10:58 PM	1.89	Bad Weather
Nov. 7	7:03 PM	1.21	Nov. 7	7:48 PM	1.33	Nov. 7	8:33 PM	1.49	Bad Weather
Nov. 12	5:39 PM	1.09	Nov. 12	6:24 PM	1.17	Nov. 12	7:09 PM	1.27	Broken CCD
Dec. 19	7:04 PM	1.94	Dec. 19	7:49 PM	2.46	Dec. 19	8:34 PM	3.07	Broken CCD
Dec. 24	5:39 PM	1.57	Dec. 24	6:24 PM	1.84	Dec. 24	7:09 PM	2.20	Broken CCD
Dec. 27	4:57 PM	3.24	Dec. 27	5:42 PM	2.46	Dec. 27	5:42 PM	2.00	Broken CCD
Feb. 7	4:58 AM	1.52	Feb. 7	5:43 AM	1.35	Feb. 7	6:28 AM	1.22	Broken CCD
Feb. 12	3:33 AM	1.94	Feb. 12	4:18 AM	1.62	Feb. 12	5:03 AM	1.41	Broken CCD
Feb. 17	2:09 AM	2.56	Feb 17	2:54 AM	2.06	Feb. 12	3:39 AM	1.74	Broken CCD
Feb. 22	12:44 AM	3.86	Feb. 22	1:29 AM	2.92	Feb. 22	2:14 AM	2.28	Broken CCD
Mar. 26	4:34 AM	1.19	Mar. 26	5:19 AM	1.11	Mar. 26	6:04 AM	1.05	...
Mar. 31	3:10 AM	1.37	Mar. 31	3:55 AM	1.24	Mar. 31	4:40 AM	1.14	...
Apr. 5	1:45 AM	1.66	Apr. 5	2:30 AM	1.44	Apr. 5	3:15 AM	1.29	...
Apr. 10	12:20 AM	1.20	Apr. 10	1:05 AM	1.79	Apr. 10	1:50 AM	1.56	...
Apr. 14	10:56 AM	3.07	Apr. 14	11:41 PM	2.37	Apr. 15	12:26 AM	1.94	...

All times before November 1, 2009 or after March 14, 2010 given in EDT. All times between November 1, 2009 and March 14, 2010 in EST.

Table 4.3: Stellar Parameters of TrES-2

Parameter	Value
RA	19 07 14
Dec	+49 18 59
Spectral Type	G0V
T_{eff}(K)	5850 ± 50
$[Fe/H]$	-0.15 ± 0.1
$M_*(M_\odot)$	0.98 ± 0.062
$R_*(R_\odot)$	1.0 ± 0.036
m_V (mag)	11.41
Age (Gyr)	5.1 ± 2.7
Distance (pc)	220 ± 10

Values from The Extrasolar Planet Encylopedia at http://www.exoplanet.edu

4.3 Analysis of TrES-2 Light Curve

I fit a single transit from the night of September 21, 2009 to a model light curve using my fitting program. The light curve is given in Figure 4.3 with the fit overlaid in blue. The parameters fitted to the system are given in Table 4.5. Comparing these results to the results of the analysis of the Holman et al. (2007) paper (given in Table 3.1) a few things jump out. First, the best fit parameters to the VVO data differ fairly substantially from the best fit parameters from the Holman et al. (2007) data. Second, the errors on the VVO data using fitted limb darkening coefficients are substantially larger than the errors on the VVO data using fixed limb darkening coefficients, though the best fit parameters are are similar to each other. Third, the errors on the VVO data using fixed limb darkening are similar to the errors using fixed limb darking on the Holman et al. (2007) data, though the best fit parameters differ from each other and this difference is not within errors.

Table 4.4: Orbital Parameters of TrES-2

Parameter	Value
Year of Discovery	2006
Period(days)	2.470614 ± 0.000001
Transit Duration(days)	0.0625
Inclination (degrees)	$83.62 \pm .14$
Eccentricity	0
$M_p(M_J)$	1.198 ± 0.053
$R_P(R_J)$	$1.220 \pm .043$
Semi major axis(AU)	0.03556

Values from Sozzetti et al. (2007) and Holman et al. (2007).

The results from the VVO data using fitted limb darkening are expected. The limb darkening coefficients primarily determine the shape of the light curve, which is quite subtle and impossible to constrain accurately without extremely precise data. Since we only have one light curve from VVO, the shape of the light curve is not well enough defined to accurately fit these coefficients, and trying to do so results in a much larger error. In contrast, Holman et al. (2007) obtain a higher quality light curve with many more points and a better defined shape. Compared to our one transit on a 24" telescope, Holman et al. (2007) observed 3 transits using a the 48" telescope at the Fred L. Whipple Observatory (FLWO) in Mt. Hopkins, Arizona. As a result, they obtained higher quality data that produced a better fit. Obtaining more light curves at VVO would provide a much better fit, and provide a better comparison to the results of Holman et al. (2007).

Unexpectedly, the errors on the best fit parameters from the VVO data for fixed limb darkening are very similar to the errors on the Holman et al. (2007) data. This is a strange result, as Holman et al. (2007) have a better light curve with many more data points, and the two fits result in substantially different values that are not within errors, particularly for R_* and R_p. This result probably

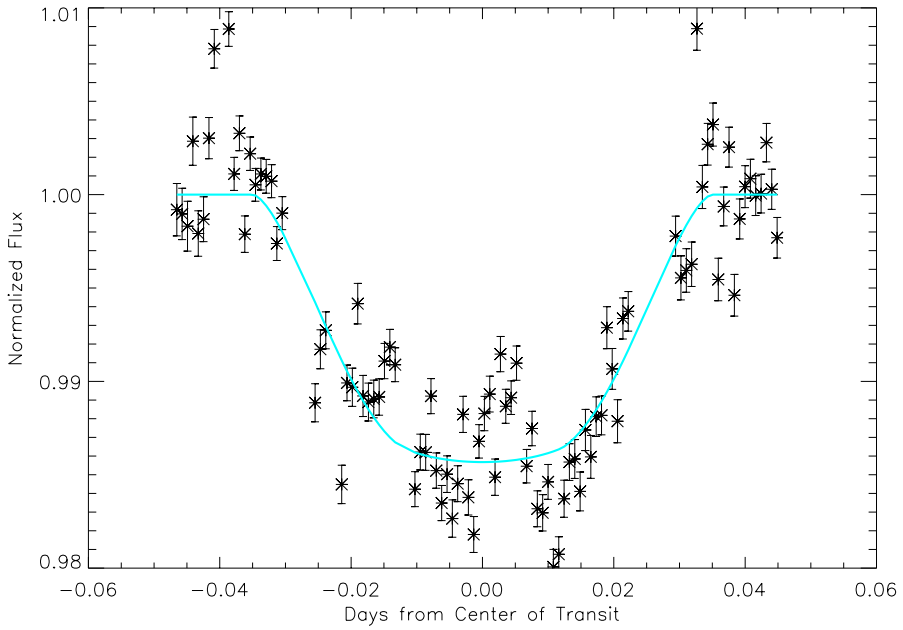

Figure 4.3: Transit light curve for TrES-2 with a fit line overlaid in blue. The fit was determined using fixed limb darkening coefficients. The light curve was obtained from VVO on September 21, 2009. The fitted parameters are given in Table 4.5.

stems from multiple causes. For one, our error analysis is not a full MCMC, and thus it is really only a rough estimate of what the errors should be. The more interesting cause, however, is that while fixing the limb darkening coefficients does not have a huge impact on the best fit values (the best fit values for fitted limb darkening and fixed limb darkening for the VVO data are very similar), it does have a large impact on the error determinations. Assuming fixed limb darkening coefficients from a model, the approach used by Holman et al. (2007) and many other papers (Southworth et al. (2007), Bakos et al. (2009), for example), is not a rigorous assumption. These are model values based on the estimates of other parameters of the system ($[Fe/H]$, $\log g$, turbulent velocity, T_{eff}) and should have

Table 4.5: Fitted System Parameters of TrES-2

Parameter	**Value**	**Error**	**Value**	**Error**
	Fitted μ_1 and μ_2		Fixed μ_1 and μ_2	
R_* ($R_\odot$)	0.9117	$\pm$0.1340	0.9035	$\pm$.0192
R_p (R_J)	1.074	$\pm$0.2175	1.085	$\pm$0.02387
p	0.1211	$\pm$0.0056	0.1234	$\pm$0.0056
i (degrees)	84.18	$\pm$1.94	84.31	$\pm$0.0174
μ_1	–0.14	$\pm$0.62	0.22 (fixed)	–
μ_2	0.61	$\pm$0.10	0.32 (fixed)	–
t_c (HJD)	2455095.59206735	$\pm$0.00023	2455095.59206796	$\pm$0.00027

Note– all of the errors were calculated using the same method outline in Section 3.0.5.

substantial errors. However, the exact errors on these model coefficients are hard to determine, and the papers that adopt these fixed limb darkening coefficients are not very forthcoming about their approaches to deal with this error. Most appear to ignore it altogether. This approach very likely results in misleadingly low error calculations. To investigate this effect further would require conducting a full MCMC as well as experimenting with different methods of evaluating the errors due to the model limb darkening coefficients.

The bottom line is that more transit light curves are necessary to provide an accurate fit of the system parameters. However, this fact is not clear from the error determinations since fixing the limb darkening coefficients ignores the error from this source. It would be a highly interesting and worthwhile future project to collect more light curves and observe the changes to the best fit values and error determinations, as well as to more rigorously explore methods of quantifying this error contribution from the limb darkening coefficients.

Chapter 5

Conclusion

The bulk of this thesis has been writing a program to fit light curves and testing its effectiveness. Comparisons of our work to the fits of Holman et al. (2007) demonstrate that the program well matches their fits. There is still some work to be done to pin down more precise errors on the fit parameters, but the result of this project has been to produce a working fitting program capable of accurately determining the parameters of transiting systems. With this program in place, it is now possible to turn attention to the ways this program can be improved, and what kind of transit observations and analysis are best suited to the facilities at Wesleyan.

5.1 Limb Darkening

One important consequence of this work is to illuminate concretely how problematic fitting limb darkening coefficients can be. This fact is certainly known by the exoplanet community, and it is evident in the literature because groups have used a wide variety of techniques to more accurately determine the limb darkening, but these difficulties are also generally glossed over and played down in published papers. Some of the techniques that other groups have used to determine limb darkening include adopting limb darkening coefficients from theoretical models, an approach we test (Bakos et al. 2009; Holman et al. 2007; Southworth et al.

2007), and fitting linear combinations of the limb darkening coefficients ($2\mu_1 + \mu_2$, $\mu_1 - 2\mu_2$, for example; Holman et al. 2006). Many papers employ both techniques in tandem, fitting the limb darkening coefficients and comparing them to model values. The reality is that the limb darkening coefficients are hard to fit because μ_1 and μ_2 are strongly dependent on each other (Mandel & Agol 2002). It is possible to produce drastically different limb darkening coefficients for the same transiting planet. It is even possible to produce drastically different limb darkening coefficients for the same light curve by very slightly tweaking the starting values given to AMOEBA. Fitting the limb darkening coefficients, even given excellent data, is very difficult. These difficulties are not adequately reflected in the error determinations.

Fitting the limb darkening coefficients directly using data taken from Van Vleck is probably impossible because, though the light curves are be able to produce are adequate, fitting the limb darkening does not work well even for higher quality data such as in Holman et al. (2007). Determining adequate limb darkening even remains a problem when analyzing Kepler data, the highest quality data we are likely to see any time soon (personal communication, Dave Latham). However, it would be an interesting project to try fitting light curves from Van Vleck using some of the other techniques employed by other groups and comparing the results. For this project we compared a fit using both fitted limb darkening coefficients and limb darkening coefficients fixed from models, but there are other approaches available. For instance, it is possible to fit a linear combination of the limb darkening coefficients (Holman et al. 2006) or to use an iterative procedure that uses both model values and fit values for the limb darkening similar to the procedure implemented by Holman et al. (2007). Comparing the results of these four methods of determining limb darkening (fixing them from models,

fitting them directly, fitting a linear combination of the two coefficients, or using an iterative procedure) would be interesting. Since most groups try to minimize the emphasis on the difficulty of fitting limb darkening coefficients, not much has been done to fully explore the differences between these methods. Figuring out the specific ways each these approaches impacts final best fit values and error determinations would be quite useful. This kind of project would be most useful when analyzing very high quality light curves like *Kepler*'s. It is probably advisable to use model values for the limb darkening when fitting light curves from Van Vleck, but more work should be done on the error analysis to provide more accurate error determinations (see Section 3.0.5).

5.2 Future Observations

Exoplanet research promises to be an exciting field in the years to come. For one, the *Kepler* mission is starting to return high precision transit data from which we can learn a lot. Of course, *Kepler* does not cover the whole sky. Ground based observations of exoplanets will continue to be useful in the years to come, and there are many potentially interesting exoplanet research projects that can be conducted at Wesleyan.

5.2.1 *Kepler*

It has been about a year since *Kepler*'s launch and the mission has started to send back data. The light curves returned by *Kepler* are not only extremely high precision (see Figure 5.1), they are also numerous and sequential because the star is continuously monitored (see Figure 5.2). With curves of a precision this high, it is quite easy to obtain a fit, even while fitting limb darkening coefficients.

Needless to say, measurements of this precision cannot be made from the ground. One need only to compare the *Kepler* light curve of TrES-2 given in Figure 5.1 to the light curve obtained at VVO (Figure 4.3) and the light curve obtained by Holman et al. (2007) (see Figure 3.1) to see how fantastic the *Kepler* data is. Undoubtedly we will learn a great deal about the number and type of exoplanets out there as *Kepler* continues to return data.

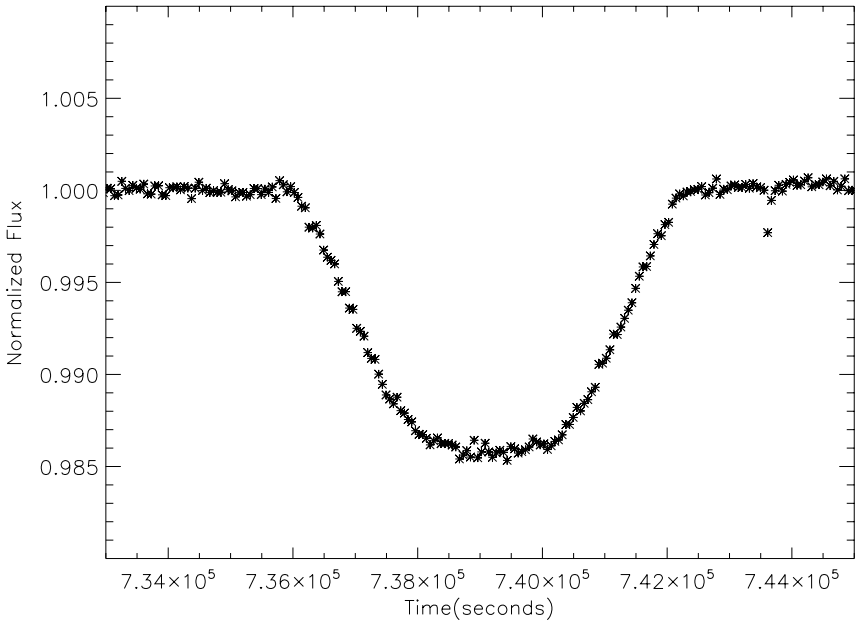

Figure 5.1: May 21, 2009 transit of the exoplanet TrES-2 from *Kepler*. Errors are within the points. Times are in seconds since the first exposure. This data was downloaded from http://archive.stsci.edu/kepler.

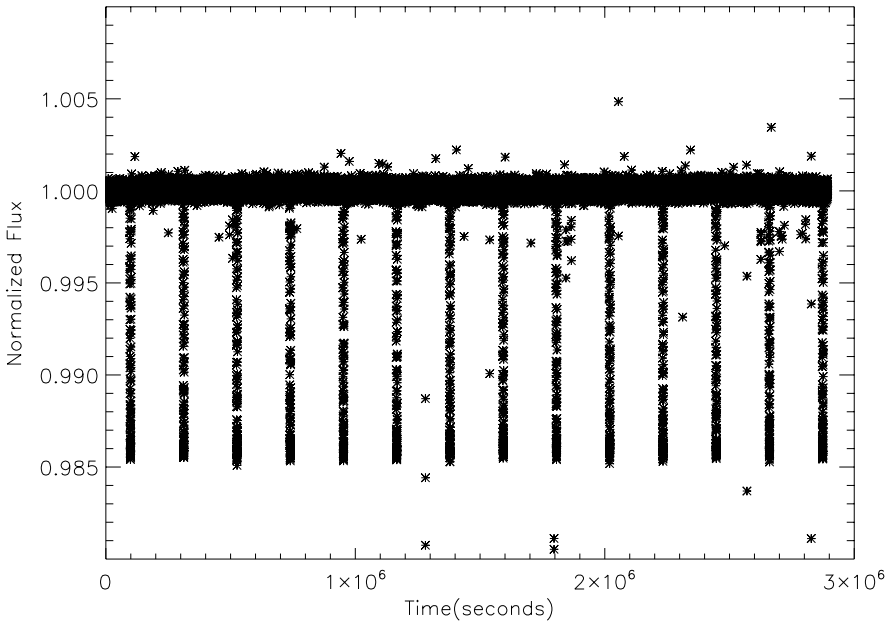

Figure 5.2: 14 consecutive transits of the exoplanet TrES-2 from *Kepler*. Times are in seconds since first exposure. The data was taken between May 13, 2009 and June 15, 2009 and downloaded from http://archive.stsci.edu/kepler.

5.2.2 Observations at Wesleyan

Now that we know it is possible to get usable data at Wesleyan it is useful to consider what kind of projects would be informative and feasible to do at Wesleyan. One such project would be exploring some other approaches to limb darkening as outlined in Section 5.1. Another would be to obtain several light curves of one (or a few) exoplanets, as was one of the initial aims of this project. One of the key points this project should illuminate is that it is entirely possible to obtain a light curve of a transiting exoplanet from Van Vleck Observatory. Though we were only able to obtain a light curve for one transit due to several instrumental problems, this one curve does demonstrate that our telescope is good enough to view transits, and that our data reduction programs are effective in producing usable light curves. It also demonstrates that, though the telescope has no autoguiding, it is possible to keep the target reasonably well centered simply by monitoring the drift and recentering periodically (see Figures 4.1 and 4.2). This measure, combined with the defocusing technique, does yield good data (see Chapter 4).

It is also apparent from this project that one light curve simply is not precise enough to obtain a good fit. Most groups fit the data from at least 3 or 4 transits simultaneously. Though this does introduce more free parameters (the transit center times for each transit), the errors in these parameters tend to be very small, and in general the more light curves the better quality the fit. It is therefore highly advisable that future efforts to observe and fit transiting exoplanets focus on obtaining multiple transits for each system. Though currently the observing program is set up to view all possible transiting systems, it would be more worthwhile to focus more intently on a few interesting systems and prioritize

their transits. Setting up a program similar to the initial observing plan outlined in Chapter 4 with a few carefully selected targets could potentially yield almost a dozen transits in a semester. Successfully observing even a quarter of these would provide enough light curves for a thorough analysis of that planetary system.

We now have data reduction programs in place and a successful fitting program to use. The stage is set for more observations to be made. We can start to push the limits of our equipment, picking smaller and fainter planetary systems than TrES-2 and seeing if it is possible to observe a transit with a shallower light curve. It should certainly be possible to do good science with this set up, constraining the parameters of newly discovered and not well understood exoplanets.

It would also be interesting to experiment with the values fit by AMOEBA. Though for this thesis we chose to fit R_*, R_p, i,t_c, μ_1, and μ_2, and assume a value for a_p (the approach used by Holman et al. (2006), there are some other options available. One possibility is to fit a_p/R_* and R_p/R_*, and from this determine values for R_* and R_p by adopting a value M_*. It is also possible to use this fitting technique to fit quantities like the flux dependence on airmass and the out of transit flux, an approach used in Holman et al. (2007). It might be useful to compare the results of fits using different free parameters and compare the results.

In conclusion, light curve analysis is far from a perfected science. Transiting exoplanets are a relatively new field, and the approaches different groups use to fit these light curves vary from paper to paper. There appears to be no clear consensus on which methods are the most accurate and effective, and groups are constantly searching for novel new fitting procedures that may further refine the information we are able to glean from transit light curves. There is much more research to be done on transiting planets in the years to come, and students and staff at Wesleyan have the facilities to make many new contributions to the field.

Bibliography

Abe, F., et al. 2004, Science, 305, 1264

Agol, E., Steffen, J., Sari, R., & Clarkson, W. 2005, MNRAS, 359, 567

Bakos, G. Á., et al. 2009, ApJ, 696, 1950

Basri, G., & Brown, M. E. 2006, Annual Review of Earth and Planetary Sciences, 34, 193

Beaulieu, J., et al. 2006, Nature, 439, 437

Bennett, D. P., et al. 2008, ApJ, 684, 663

Bennett, D. P., & Rhie, S. H. 1996, ApJ, 472, 660

Bevington, P. R., & Robinson, D. K. 1992, Data Reduction and Error Analysis for the Physical Sciences (New York: McGraw-Hill)

Borucki, W. J., et al. 2010, ArXiv e-prints

Carroll, B. W., & Ostlie, D. A. 2007

Charbonneau, D., Brown, T. M., Latham, D. W., & Mayor, M. 2000, ApJ, 529, L45

Charbonneau, D., Brown, T. M., Noyes, R. W., & Gilliland, R. L. 2002, ApJ, 568, 377

Claret, A. 2000, A&A, 363, 1081

Daemgen, S., Hormuth, F., Brandner, W., Bergfors, C., Janson, M., Hippler, S., & Henning, T. 2009, A&A, 498, 567

Doyle, L. R. 2008, in Extrasolar Planets, ed. H. Deeg, J. A. Belmonte, & A. Aparicio, 1–+

Fischer, D., et al. 2009, ApJ, 703, 1545

Ford, E. B. 2006, ApJ, 642, 505

Hastings, C. 1955, Approximations for Digital Computers (Princeton, NJ, USA: Princeton University Press)

Holman, M. J., et al. 2006, ApJ, 652, 1715

—. 2007, ApJ, 664, 1185

Kalas, P., et al. 2008, Science, 322, 1345

Léger, A., et al. 2009, A&A, 506, 287

Mandel, K., & Agol, E. 2002, ApJ, 580, L171

Marois, C., Macintosh, B., Barman, T., Zuckerman, B., Song, I., Patience, J., Lafrenière, D., & Doyon, R. 2008, Science, 322, 1348

Mayor, M., & Queloz, D. 1995, Nature, 378, 355

O'Donovan, F. T., Charbonneau, D., & Hillenbrand, L. 2006, in Bulletin of the American Astronomical Society, Vol. 38, Bulletin of the American Astronomical Society, 1212–+

Pál, A., & Bakos, G. Á. 2006, PASP, 118, 1474

Press, W. H., Teukolsky, S. A., Vetterling, W. T., & Flannery, B. P. 2007, Numerical Recipes 3rd Edition: The Art of Scientific Computing (New York, NY, USA: Cambridge University Press)

Schneider, J. 2010, The Extrasolar Planets Encyclopaedia

Snellen, I. A. G., et al. 2009, A&A, 497, 545

Southworth, J., Wheatley, P. J., & Sams, G. 2007, MNRAS, 379, L11

Sozzetti, A., Torres, G., Charbonneau, D., Latham, D. W., Holman, M. J., Winn, J. N., Laird, J. B., & O'Donovan, F. T. 2007, ApJ, 664, 1190

West, R. G., et al. 2009, A&A, 502, 395

Winn, J. N., et al. 2008, ApJ, 682, 1283

Wolszczan, A. 1992, LPI Contributions, 781, 53